Article

Cell Host & Microbe

Human gut bacterial metabolism drives Th17 activation and colitis

Graphical abstract

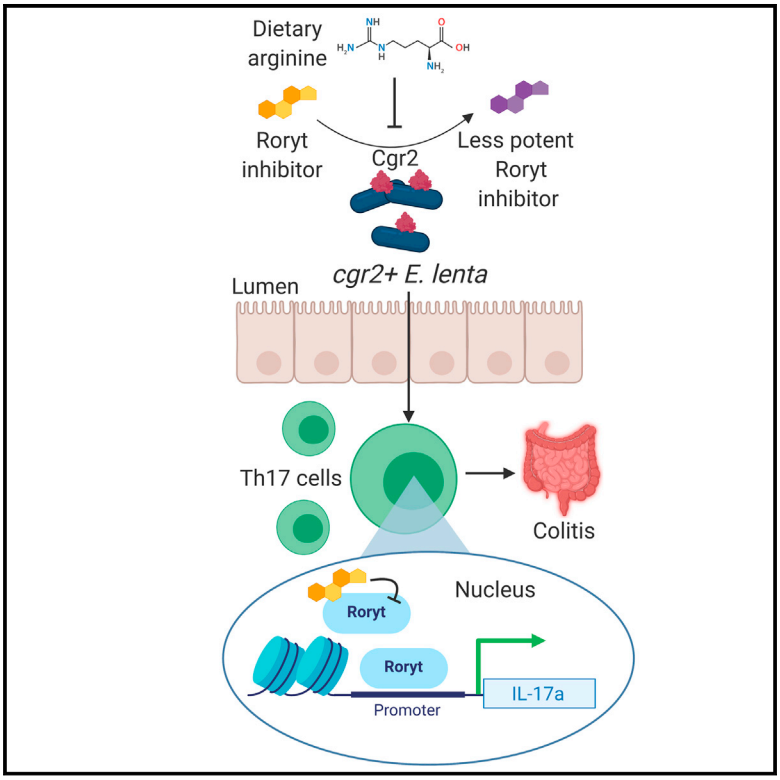

Authors

Margaret Alexander, Qi Yan Ang, Renuka R. Nayak, ..., Katherine S. Pollard, Susan V. Lynch, Peter J. Turnbaugh

Correspondence

peter.turnbaugh@ucsf.edu

In brief

Alexander et al. show an autoimmune-associated microbe, *Eggerthella lenta*, activates Th17 cells and worsens mouse models of colitis. Using strain-level variation, comparative genomics, and bacterial genetics they demonstrate that the cardiac glycoside reductase 2 (Cgr2) enzyme is sufficient for Th17 activation and that elevated dietary arginine blocks *E. lenta*-induced colitis.

Highlights

- The prevalent gut Actinobacterium *Eggerthella lenta* activates Th17 cells
- *E. lenta* is associated with human disease and exacerbates colitis in mice
- A strain-specific enzyme Cgr2 induces IL-17a via the metabolism of Rorγt inhibitors
- Dietary arginine blocks *E. lenta*-induced intestinal inflammation

Alexander et al., 2022, Cell Host & Microbe *30*, 17–30
January 12, 2022
https://doi.org/10.1016/j.chom.2021.11.001

CellPress

Cell Host & Microbe

CellPress
OPEN ACCESS

Article

Human gut bacterial metabolism drives Th17 activation and colitis

Margaret Alexander,[1] Qi Yan Ang,[1] Renuka R. Nayak,[1,2] Annamarie E. Bustion,[3] Moriah Sandy,[1,2] Bing Zhang,[2] Vaibhav Upadhyay,[1,2] Katherine S. Pollard,[3,4,5] Susan V. Lynch,[2] and Peter J. Turnbaugh[1,6,*]

[1]Department of Microbiology & Immunology, University of California San Francisco, San Francisco, CA 94143, USA
[2]Department of Medicine, University of California, San Francisco, San Francisco, CA 94158, USA
[3]Gladstone Institutes, San Francisco, CA 94158, USA
[4]Chan Zuckerberg Biohub, San Francisco, CA 94158, USA
[5]Department of Epidemiology and Biostatistics, University of California San Francisco, San Francisco, CA 94158, USA
[6]Lead contact
*Correspondence: peter.turnbaugh@ucsf.edu
https://doi.org/10.1016/j.chom.2021.11.001

SUMMARY

Bacterial activation of T helper 17 (Th17) cells exacerbates mouse models of autoimmunity, but how human-associated bacteria impact Th17-driven disease remains elusive. We show that human gut Actinobacterium *Eggerthella lenta* induces intestinal Th17 activation by lifting inhibition of the Th17 transcription factor Rorγt through cell- and antigen-independent mechanisms. *E. lenta* is enriched in inflammatory bowel disease (IBD) patients and worsens colitis in a *Rorc*-dependent manner in mice. Th17 activation varies across *E. lenta* strains, which is attributable to the cardiac glycoside reductase 2 (Cgr2) enzyme. Cgr2 is sufficient to induce interleukin (IL)-17a, a major Th17 cytokine. *cgr2*+ *E. lenta* deplete putative steroidal glycosides in pure culture; related compounds are negatively associated with human IBD severity. Finally, leveraging the sensitivity of Cgr2 to dietary arginine, we prevented *E. lenta*-induced intestinal inflammation in mice. Together, these results support a role for human gut bacterial metabolism in driving Th17-dependent autoimmunity.

INTRODUCTION

Intestinal immune responses are linked to the trillions of microorganisms that colonize the gastrointestinal tract (Belkaid and Hand, 2014). Thus, inter-individual variations in the gut microbiome have been hypothesized to broadly impact immune-related diseases (Yurkovetskiy et al., 2015). Consistent with this hypothesis, multiple disease models are ameliorated in germ-free (GF) or antibiotic-treated mice (Lee et al., 2011; Maeda et al., 2016). Microbiome-wide association studies have identified bacteria enriched in autoimmune diseases, including rheumatoid arthritis (RA), inflammatory bowel disease (IBD), and multiple sclerosis (MS) (Cekanaviciute et al., 2017; Frank et al., 2007; Zhang et al., 2015). Yet, the key players and their causal role in disease remain largely unknown. Furthermore, as the complex interplay between diet, microbiome, and immune responses is becoming more apparent (Alexander and Turnbaugh, 2020), more work is needed to elucidate the mechanisms of these interactions and their disease relevance.

Bacterial activation of Th17 cells exacerbates mouse models of autoimmunity; yet, the diverse mechanisms of how autoimmune-associated bacteria contribute to Th17 activation and disease are still being elucidated. Seminal work revealed that segmented filamentous bacteria (SFB) increase Th17 cells in mice (Atarashi et al., 2015; Ivanov et al., 2009). Likewise, bacterial communities and isolates from IBD stool impact Th17 levels and disease severity following transfer into GF mice (Britton et al., 2019, 2020). In humans, specific bacterial and fungal members of the microbiota have been implicated in Th17 induction. *Candida albicans* colonization activates fungal-specific Th17 induction (Bacher et al., 2019; Shao et al., 2019). A broad range of members of the microbiota have been screened for their Th17-inducing capacity (Tan et al., 2016). In these studies, a select few bacterial species promote Th17 induction. Among these was the prevalent Actinobacterium *Bifidobacterium adolescentis*, which increased Th17 cells in an antigen-specific manner and worsened arthritis in mice. Similar to SFB, the physical adhesion of *B. adolescentis* to the intestinal epithelium has been implicated in the mechanism of Th17 induction; however, other autoimmune-associated gut bacterial species may regulate Th17 cells and influence autoimmunity through adhesion- and/or antigen-independent mechanisms such as the metabolism of immunomodulatory substrates.

Here, we demonstrate that the metabolic activity of human gut bacteria promotes Th17 activation exacerbating colitis severity. We focused on the prevalent human Actinobacterium *Eggerthella lenta* due to (1) our prior work on digoxin (a cardiac drug metabolized by *E. lenta* that also inhibits the Th17 master transcription factor Rorγt) (Haiser et al., 2013; Huh et al., 2011), (2) the phylogenetic relationship between *E. lenta* and the Th17-inducing *B. adolescentis*, and (3) emerging evidence that *E. lenta* is enriched in patients spanning multiple autoimmune diseases (Cekanaviciute et al., 2017; Zhang et al., 2015; Zhu et al., 2021). Our results add *E. lenta* to the growing list of immunomodulatory microorganisms relevant to IBD and emphasize the importance of considering

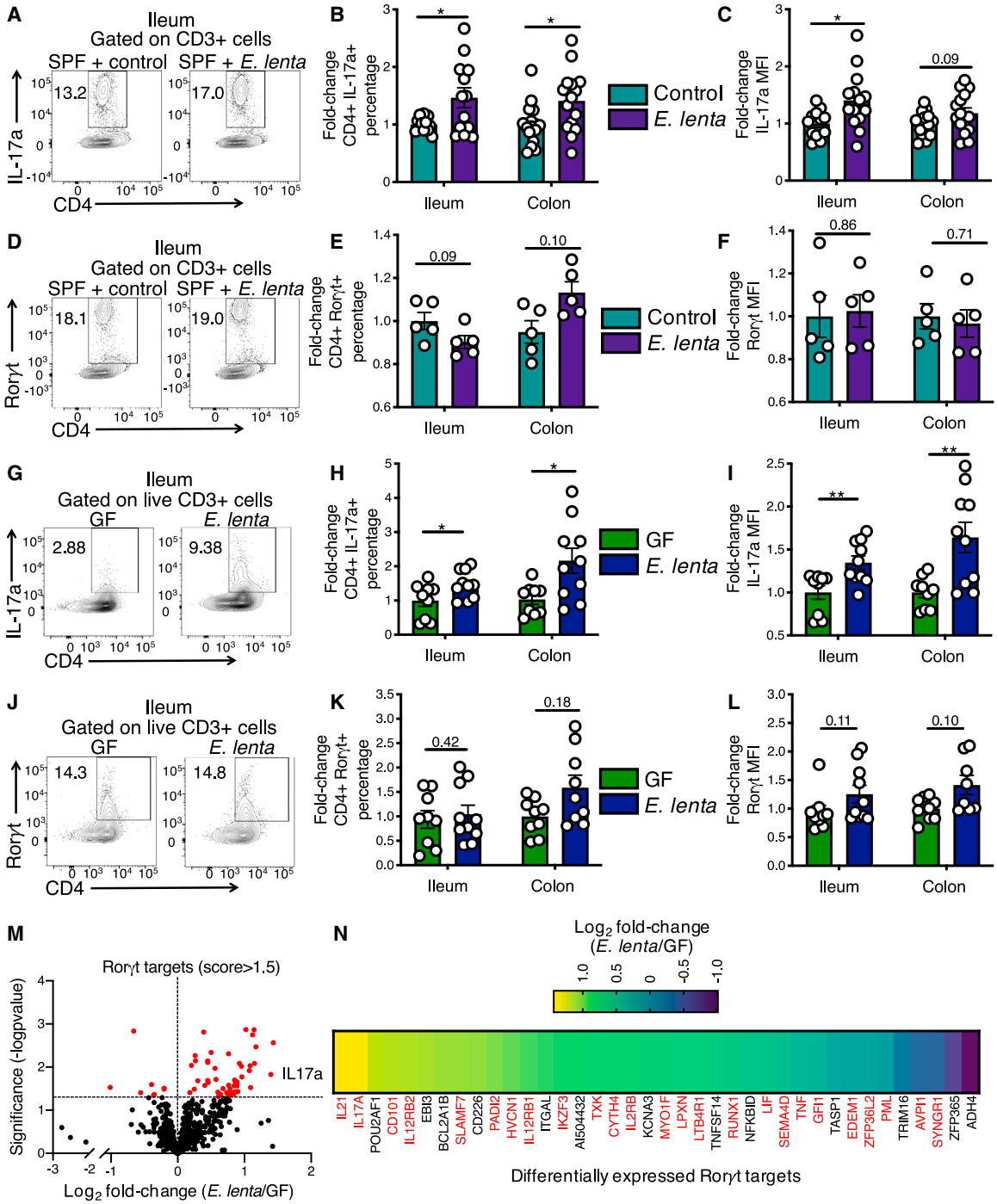

Figure 1. *E. lenta* colonization promotes intestinal Th17 activity in the presence and absence of the gut microbiota

(A–F) C57BL/6J SPF mice were gavaged every other day for 2 weeks with BHI media control or *E. lenta* 2243. (A) Representative ileal flow plots, (B) fold-change IL-17a+ $CD4^+$ cells within the $CD3^+$ gate, (C) IL-17a mean fluorescence intensity (MFI) in the ileal and colonic lamina propria (LP) (n = 15). Data from three independent experiments. (D) Representative ileal flow plots, (E) fold-change of Rorγt+ $CD4^+$ cells within $CD3^+$ gate, (F) Rorγt MFI in the ileal and colonic LP (n = 5). Fold-change is relative to BHI. Data from one experiment.

(G–L) Germ-free (GF) mice were colonized with *E. lenta* 2243 for 2 weeks or remained GF. (G) Representative ileal flow plots, (H) fold-change of IL-17a+ $CD4^+$ cells within the live $CD3^+$ gate, (I) IL-17a MFI in the ileal and colonic LP (n = 8–10). (J) Representative ileal flow plots, (K) fold-change of $CD4^+$ Rorγt+ cells within the live $CD3^+$ gate, (L) MFI of Rorγt in the ileal and colonic LP (n = 8–10). Data from one representative experiment. Fold-change relative to GF. Each point represents an individual mouse, mean ± SEM plotted in (A–L). *p < 0.05; **p < 0.01; listed, Welch's t test.

(legend continued on next page)

the impact of strain-specific microbial metabolism on immune responses and autoimmunity.

RESULTS

E. lenta promotes Th17 activity in the presence or absence of the gut microbiota

Due to *E. lenta* associations with autoimmune diseases connected to aberrant Th17 activity, we sought to determine if *E. lenta* impacts Th17 cells in mice that had been colonized their entire life with a complex gut microbiota. We gavaged specific pathogen-free (SPF) mice with the *E. lenta* type strain (DSM 2243) or a BHI (brain heart infusion media) control every other day for 2 weeks and confirmed *E. lenta* presence with qPCR (Figure S1A). IL-17a$^+$ CD4$^+$ cells (Th17) in the ileal and colonic lamina propria were significantly increased compared with BHI in fold-change, cell percentages, and absolute numbers (Figures 1A and 1B; Data S1 and S2). IL-17a mean fluorescence intensity (MFI) was significantly increased in response to *E. lenta* (Figure 1C). We observed similar patterns in the IL-17f$^+$ CD4$^+$ population and IL-17f MFI but no significant differences in the CD4$^+$ Rorγt+ population (Figures S1B–S1D and 1D–1F). These results indicate that while CD4$^+$ Rorγt$^+$ levels are not altered by *E. lenta*, the expression of Rorγt targets IL-17a and IL-17f are elevated. Further, our findings demonstrate that *E. lenta* impacts Th17 activity in the presence of an intact microbiota.

To assess if *E. lenta* colonization is sufficient to increase Th17 activity in the absence of a background gut microbiota we monocolonized GF mice with *E. lenta* 2243 for 2 weeks. *E. lenta* monocolonized mice had increased fold-change, percentages, and numbers of IL-17a$^+$ CD4$^+$ cells as well as elevated IL-17a MFI in the ileum and colon but not spleen compared with GF (Figures 1G–1I, S1E, and S1F; Data S1 and S2). CD4$^+$ Rorγt$^+$ levels and Rorγt MFI were not altered in *E. lenta* colonized mice (Figures 1J–1L, S1G, and S1H). *E. lenta* monocolonization did not significantly impact intestinal IFNγ^+ CD4$^+$ T cells, IL17a$^+$ TCR$\gamma\delta^+$ T cells, or lineage- Rorγt$^+$ IL-17a$^+$ group 3 innate lymphoid cells (ILC3) (Figures S1I–S1P; Data S1 and S2). Thus, *E. lenta* impacts Th17 function irrespective of the presence of other gut microbes.

To broadly assess changes in gene expression in CD4$^+$ T cells in *E. lenta* monocolonized mice compared with GF, we performed RNA-seq on isolated ileal lamina propria CD4$^+$ cells. This analysis revealed a significant enrichment of Th17 genes and Rorγt targets (Ciofani et al., 2012) in response to *E. lenta* colonization (Figures 1M, 1N, and S1Q; Table S1; p value $<10^{-6}$, hypergeometric test). RT-qPCR of GF and *E. lenta* monocolonized mice ileal tissue confirmed a significant increase in Rorγt targets IL-17f and CCR6 (Figure S1R). There were no significant changes in regulatory T cell (Treg)-associated transcript (Foxp3), T helper 1 (Th1)-associated transcripts (IFNγ, Tbet), or other inflammatory markers (Figure S1R). These results reveal that *E. lenta* colonization specifically induces Rorγt targets.

E. lenta induces IL-17 in an antigen-independent manner by lifting Rorγt inhibition

To test if *E. lenta* shapes Th17 cell function by changing soluble immunomodulatory molecules, we orally gavaged SPF mice with the small molecule (<3 kDa) fraction of 2× concentrated cell-free supernatant (CFS), media controls, or heat-killed *E. lenta* cells (Figure 2A). CFS led to significant increases in intestinal Th17 cells (Figures 2B and 2C) and IL-17a MFI (Figure 2D). CD4$^+$ IL-17f$^+$ cells and IL-17f MFI levels were increased in the ileum of CFS-treated mice (Figures S3A–S3C). Heat-killed *E. lenta* did not significantly alter CD4$^+$ IL-17a$^+$ or IL-17f$^+$ cells or IL-17a or IL-17f levels (Figures 2B–2D and S3A–S3C). These findings suggest that metabolically active *E. lenta* induce IL-17a and IL-17f by impacting immunomodulatory small molecules.

To further explore the presence of soluble immunomodulatory molecules, we used an *in vitro* assay. Th17 skewed splenic CD4$^+$ T cells were treated with CFS from *E. lenta* 2243 or controls (Figure 2E). Untreated, heat-treated, or 3 kDa filtered CFS significantly increased IL-17a compared with controls (Figures 2F, S3D, and S3E; Data S3). BHI media significantly decreased IL-17a production, providing initial support for the presence of an inhibitor of IL-17a expression in the media that is counteracted by *E. lenta* growth (Figures 2F, S3D, and S3E).

Our mouse experiments indicated that *E. lenta* acts downstream of Th17 differentiation and proliferation. To address this *in vitro*, we added *E. lenta* 2243 CFS to the Th17 *in vitro* assay at multiple time points, either at the same time or 4 days after skewing (Figure 2E). CFS resulted in significantly higher IL-17a levels at both time points (Figure 2G) with no significant differences in proliferation (Figure 2H). These results reveal that *E. lenta* CFS impacts IL-17a production after cells have been differentiated without significant impacts on proliferation. Based on these findings, we predicted that *E. lenta* could rapidly increase Th17 activation prior to an adaptive immune response, consistent with a short-term monocolonization experiment that significantly increased intestinal Th17 levels and IL-17a MFI (Figures S3G–S3K). Finally, using a Rorγ luciferase assay, we found that BHI significantly decreased Rorγ activity similar to a known Rorγt inhibitor ursolic acid, while CFS had no effect (Figures 2I, 2J, and S3F). These data indicate that a Rorγt inhibitor present in BHI media is metabolized by *E. lenta* into a less potent inhibitor.

Our results indicate that the Th17 response to *E. lenta* is not due to a specific antigen, in contrast to prior work on enteric bacteria (Goto et al., 2014; Tan et al., 2016) and fungi (Bacher et al., 2019). To test antigen specificity, we treated SPF mice with BHI media (− control), *E. lenta* 2243, or *B. adolescentis* BD1 (+ control) for 2 weeks before ileal CD4$^+$ T cells were isolated and challenged with mock (BHI)-, *E. lenta*-, or *B. adolescentis*-loaded dendritic cells (DCs) (Figure 2K). T cells isolated from mice treated with *E. lenta* had significantly elevated Th17 levels

(M and N) RNA-seq of ileal LP CD4$^+$ cells from GF or *E. lenta* monocolonized mice (n = 4). (M) Volcano plot of Rorγt targets defined by transcription-target interactions (score >1.5) (Ciofani et al., 2012). Red dots are significantly ($p < 0.05$; Wald test) differentially expressed between *E. lenta* monocolonized and GF mice. (N) Heatmap of significantly different Rorγt target transcripts ($p < 0.05$; Wald test). Transcripts in red are increased in Th17 versus Th0 as in (Ciofani et al., 2012) (fold increase of >1.5 (Th17/Th0)).
See Figures S1 and S2 and Data S1 and S2.

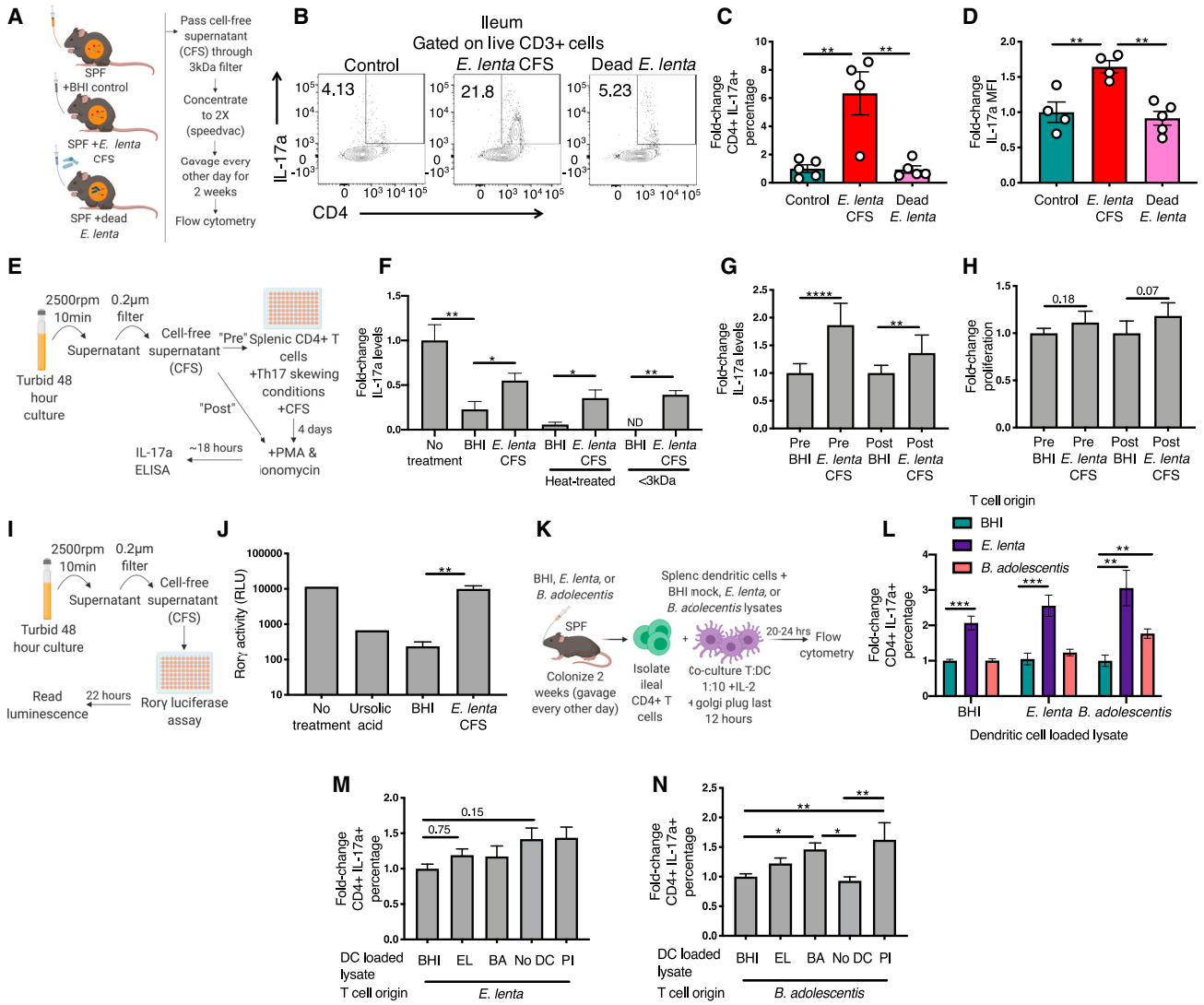

Figure 2. *E. lenta* induces IL-17a in an antigen-independent manner by lifting Rorγt inhibition

(A–D) (A) C57BL/6J SPF mice were gavaged for 2 weeks with BHI (control), *E. lenta* 2243-cell-free supernatant (CFS), or heat-killed *E. lenta* 2243 (dead). BHI and CFS were 3 kDa filtered and 2× concentrated. (B) Representative flow plots. (C) fold-changes of IL-17a$^+$ CD4$^+$ cells within the live CD3$^+$ gate. (D) IL-17a MFI in the ileum (relative to control) (n = 4–5). Data from one experiment.

(E–H) (E) *In vitro E. lenta* CFS Th17 assay design. (F) Fold-change in IL-17a levels (relative to no treatment) measured via ELISA from Th17 skewed cells that received no treatment, BHI, *E. lenta* CFS, heat-treated BHI or *E. lenta* CFS, <3 kDa filtered BHI or *E. lenta* CFS (n = 4–8). (G) Fold-change in IL-17a levels as measured by ELISA when treatments were added pre- or post-skewing. (n = 14). (H) Fold-change in proliferation levels (relative to BHI) as quantified by MTT assay from the pre and post CFS treatment (n = 9). Data from two independent experiments. p values are Welch's t tests.

(I and J) (I) Rorγ luciferase assay where Rorγ luciferase reporter cells were treated with BHI or *E. lenta* 2243 CFS at 0.625× concentration (n = 5), ursolic acid at 667 nM as a positive control of a Rorγ inhibitor (n = 2), or no treatment (n = 2). (J) Rorγ activity as measured by luminescence—relative light unit (RLU).

(K–N) (K) Antigen specificity experimental design. (L) Relative IL-17a$^+$ CD4$^+$ levels within the live CD3$^+$ gate as assessed by flow cytometry (levels relative to BHI T cell control). Data are from 2 independent experiments (n = 10–12). (M) Fold-change in CD4$^+$ IL-17a$^+$ cells within the live CD3$^+$ population from T cells isolated from SPF mice colonized with *E. lenta* and co-cultured with dendritic cells (DCs) loaded with lysates from BHI, *E. lenta*, *B. adolescentis*, no DCs or PMA/ionomycin (PI). Levels are relative to BHI. (N) Fold-change in CD4$^+$ IL-17a$^+$ cells within the live CD3$^+$ population from T cells isolated from SPF mice colonized with *B. adolescentis* and co-cultured with DCs loaded with lysates from BHI, *E. lenta*, *B. adolescentis*, no DCs or PI. Levels are relative to the BHI control.

*p < 0.05; **p < 0.01; ***p < 0.001; ****p < 0.0001; listed; one-way ANOVA with Tukey or Holm Sidak tests unless otherwise stated. Mean ± SEM is displayed. Model figures made with BioRender.com. See also Figures S2 and S3 and Data S3.

compared with T cells from mice treated with BHI or *B. adolescentis* independent of DC lysate and presence of dendritic cells (Figures 2L and 2M). Consistent with previous reports (Tan et al., 2016), *B. adolescentis* conditioned T cells only produced elevated IL-17a levels when challenged with *B. adolescentis*-loaded DCs (Figure 2N). These findings suggest that *E. lenta* programs elevated IL-17a levels independent of antigen presentation, which may explain the broad associations of this bacterial species across multiple autoimmune diseases with distinct antigenic stimuli.

E. lenta is associated with inflammatory bowel disease and contributes to colitis in a *Rorc*-dependent manner

Prior studies have detected *E. lenta* at higher levels in disease states associated with aberrant Th17 activation relative to healthy controls, including RA (Zhang et al., 2015) and MS (Cekanaviciute et al., 2017). To test if *E. lenta* is also enriched in IBD patients, we re-analyzed two metagenomic datasets totaling 105 IBD patients and 100 healthy subjects (Qin et al., 2010; Weng et al., 2019). *E. lenta* was significantly higher in IBD patient stool samples relative to controls (Figures 3A, 3B, and S4A–S4C). *E. lenta* levels were also elevated in IBD states compared with controls in an independent IBD cohort (Figure S4D). With previous studies, these findings indicate that *E. lenta* is elevated in a range of autoimmune diseases, revealing a broad association of *E. lenta* with autoimmunity.

Next, we used mouse models of IBD to test the impact of *E. lenta* colonization on disease severity. First, GF mice were colonized for 2 weeks with *E. lenta* prior to dextran sodium sulfate (DSS) colitis induction (Figure 3C). *E. lenta* colonized mice developed more severe disease than GF by multiple metrics: disease score, colon length, crypt destruction as observed via histology, and colonic lipocalin levels (Figures 3D–3G and S4E). We observed increased colonic and ileal Th17 levels in response to *E. lenta* (Figures S4F and S4G), which negatively correlated with colon length (Figure S4H). Second, we gavaged *IL-10*$^{-/-}$ SPF mice with *E. lenta* or a media control (BHI) three times a week tracking weight and survival (Figure 3H). *E. lenta* significantly impacted multiple disease metrics including decreased body weight, decreased survival, and increased colonic lipocalin levels compared with controls (Figures 3I–3K).

These results, and our previous findings that *E. lenta* colonization impacts expression of Rorγt targets, led us to hypothesize that *E. lenta* contributes to colitis by inducing the expression of Rorγt-dependent genes. To test this hypothesis, we compared wild-type (*WT*) and *Rorc*$^{-/-}$ SPF mice gavaged with *E. lenta* or a BHI media control every other day for 2 weeks preceding DSS (Figure 3L). *E. lenta* induced more severe disease in WT mice, as assessed by disease score and colon length (Figures 3M and 3N). In contrast, *Rorc*$^{-/-}$ mice had no significant differences in disease severity between groups (Figures 3O and 3P). Th17 levels were elevated in the ileum and colon of WT mice gavaged with *E. lenta* (Figures S4I and S4J) but low for both groups in *Rorc*$^{-/-}$ mice (Figures S4K and S4L). Colonic Th17 levels negatively correlated with colon length in WT mice (Figure S4M). While we cannot exclude some contribution of additional cell types missing from *Rorc*$^{-/-}$ mice (e.g., ILC3 cells) or broader defects in thymopoiesis (Guo et al., 2016), these results are consistent with the hypothesis that *E. lenta* contributes to worsened colitis in a *Rorc*-dependent manner. Additional studies are warranted in CD4-cre *Rorc*$^{fl/fl}$ mice to assess the CD4-cell-specific impact of *E. lenta* on *Rorc* during colitis.

Th17 activation and colitis severity varies between *E. lenta* strains

To determine if Th17 activation is conserved within the *E. lenta* species, we colonized GF mice with *E. lenta* 2243 and 3 additional strains selected based on genetic distances to allow for genomic similarities and differences. Similar to *E. lenta* 2243, AB12 had a trending increase in Th17 cells in the ileum (Figures 4A and 4B) and significantly higher colon levels (Figures 4C and 4D). In contrast, there was no significant impact of 15644, 1356, or heat-killed 2243 on Th17 cells relative to GF (Figures 4A–4D and S5B). We confirmed strain-level differences in SPF mice where IL-17aGFP reporter mice treated with 2243 had significantly elevated Th17 cells compared with BHI and 1356 (Figures S5C and S5D). These strain-level differences resulted in a significant difference in colitis severity (Figures 4E–4H). Monocolonization with 2243 led to more severe colitis as measured by disease score, colon length, and fecal lipocalin compared with GF while 1356 monocolonization disease metrics were not different, consistent with strain differences in Th17 induction (Figures 4E–4H and S5F). Colonization levels were equivalent between strains (Figures S5A and S5E), suggesting that these differences are driven by the host response to these strains, not their ability to colonize the GI tract.

The gut bacterial drug metabolizing enzyme Cgr2 is associated with and sufficient for IL-17a induction

To more broadly assess the variation between the immunomodulatory potential of *E. lenta* strains, we returned to the *in vitro* Th17 assay. Compared with BHI treatment, *E. lenta* 2243 CFS significantly increased IL-17a levels while 1356 and 15644 CFS did not (Figures S6A–S6C; Data S3). We then tested a broader panel of 10 *E. lenta* strains for IL-17a induction, which revealed 4 IL-17a-inducing and 6 non-inducing strains compared with a control (Figure 5A). Using the ElenMatchR comparative genomic tool (Bisanz et al., 2020), we identified a single genomic locus matching the pattern of Th17 activation (Figure 5A). These 7 genes are within the *cgr*-associated gene cluster (*cac*) (Figure 5B), which is necessary for the metabolism of the cardiac drug digoxin and other cardenolides (Koppel et al., 2018). Further, we validated that treatment of SPF mice with CFS from a *cac*+ and a *cac*− strain showed similar results *in vivo* (Figures S6D and S6E). These results indicated that one or more of the genes in this locus also plays a role in shaping host immunity.

Prior studies showed that digoxin inhibits Rorγt leading to decreased Th17 levels by directly binding to Rorγt (Fujita-Sato et al., 2011; Huh et al., 2011). We hypothesized that the enzyme sufficient for digoxin reduction, Cgr2 (found within *cac*), could lift Rorγt inhibition by metabolizing an as-of-yet unidentified substrate found in media and the GI tract. A key prediction of this hypothesis is that Cgr2 should be sufficient to promote IL-17a. We used constructs in which WT *cgr2* or a partial loss-of-function variant of *cgr2* (Y333N) were expressed in *Rhodococcus erythropolis* under a thiostrepton-inducible promoter (Koppel et al., 2018). Expression of *cgr2*:*WT* resulted in a significant increase in IL-17a levels compared with uninduced or BHI controls (Figure 5C). There was no significant impact of *cgr2*:Y333N (Figure 5C). This was surprising, as naturally occurring *E. lenta* strains carrying the Y333N mutation (AB12 and AB8) induced IL-17a. Differences in expression levels of *cgr2* Y333N from our heterologous system and naturally occurring strains could account for this discrepancy. To address this issue, we moved to an *in vivo* system with repeated application of CFS to elevate the concentration.

To test if *cgr2* is sufficient to increase IL-17a levels *in vivo*, we treated SPF mice with CFS every other day for 2 weeks from *R. erythropolis* expressing *cgr2*:*WT* or *cgr2*:Y333N +/− the

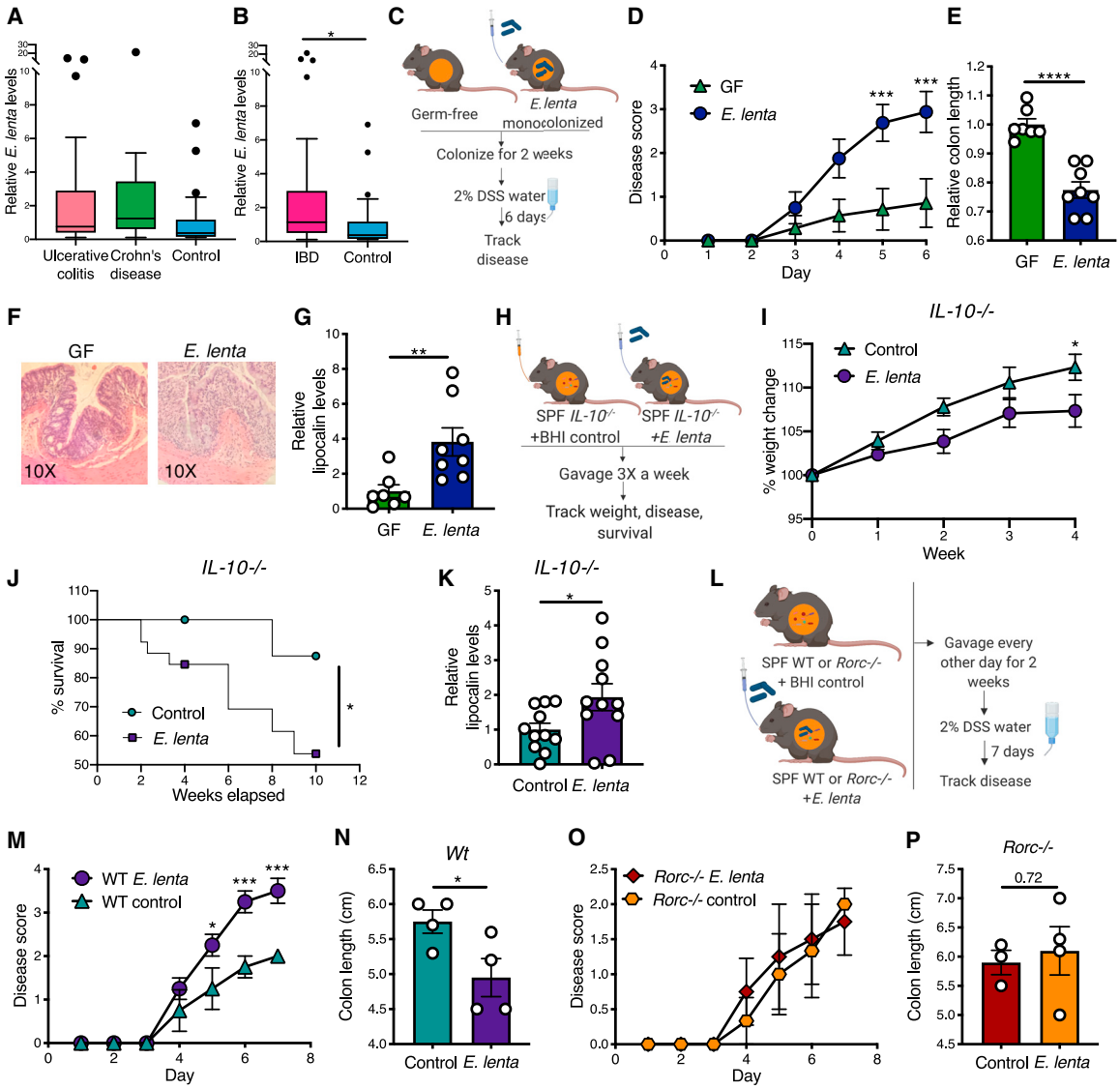

Figure 3. *E. lenta* is associated with inflammatory bowel disease and contributes to colitis in a *Rorc*-dependent manner

(A and B) Abundance of *E. lenta* was assessed using metagenomic intra-species diversity analysis system (MIDAS) to map metagenomic reads to isolate genomes and metagenome assembled genomes from the human gut environment (Almeida et al., 2019; Nayfach et al., 2016). (A) Relative abundance of *E. lenta* from studies of ulcerative colitis (UC) (n = 52), Crohn's disease (CD) (n = 53), and controls (n = 100) (Qin et al., 2010; Weng et al., 2019). Species reads were normalized by the total number of reads across species in the sample then set relative to control. (B) Relative abundance of *E. lenta* in IBD (Crohn's disease and ulcerative colitis patients combined) and control samples ($p = 0.04$, t test on the glm coefficient).

(C–G) Germ-free (GF) or *E. lenta* strain 2243 monocolonized mice (colonized for 2 weeks) were treated with 2% dextran sulfate sodium (DSS) for 6 days, and (D) disease was scored based on published scoring metrics (Chassaing et al., 2014). p values are two-way ANOVA with Sidak test. Data are from 2 independent experiments (n = 7–8). (E) Relative colon length (relative to GF). (F) Representative histology from GF or *E. lenta* monocolonized colons with H&E staining at 10× magnification. (G) Relative lipocalin levels as measured via ELISA in colon content.

(H–K) *IL-10*$^{-/-}$ SPF mice were gavaged with a BHI media or *E. lenta* 2243 three times a week for 6 weeks and (I) percentage of initial weight was tracked (n = 11). p values are two-way ANOVA with Sidak test. (J) Percent survival of *IL-10*$^{-/-}$ mice gavaged with BHI or *E. lenta* 2243 three times a week for 10 weeks (n = 19–26). Data are from 2 independent experiments. p value is a log-rank Mantel-Cox test. (K) Lipocalin levels were measured via ELISA in colon content after 6–10 weeks of gavage. Data are from 2 independent experiments and set relative to BHI (n = 11).

(L–P) SPF WT or *Rorc*$^{-/-}$ mice were gavaged with a BHI media or *E. lenta* 2243 every other day for 2 weeks then treated with 2% DSS for 7 days. (M) Disease scores over time in WT SPF mice treated with BHI or *E. lenta*. p values are two-way ANOVA with Sidak test (n = 4). (N) Day 7 colon lengths. (O) Disease scores over time in *Rorc*$^{-/-}$ SPF mice treated with BHI or *E. lenta*. (P) Day 7 colon lengths. Data are from 1 experiment.

*p < 0.05; **p < 0.01; ***p < 0.001; ****p < 0.0001; listed; Welsh's t tests unless otherwise stated.

Mean ± SEM is displayed. Each dot represents an individual mouse. Model figures made with BioRender.com. See also Figures S2 and S4.

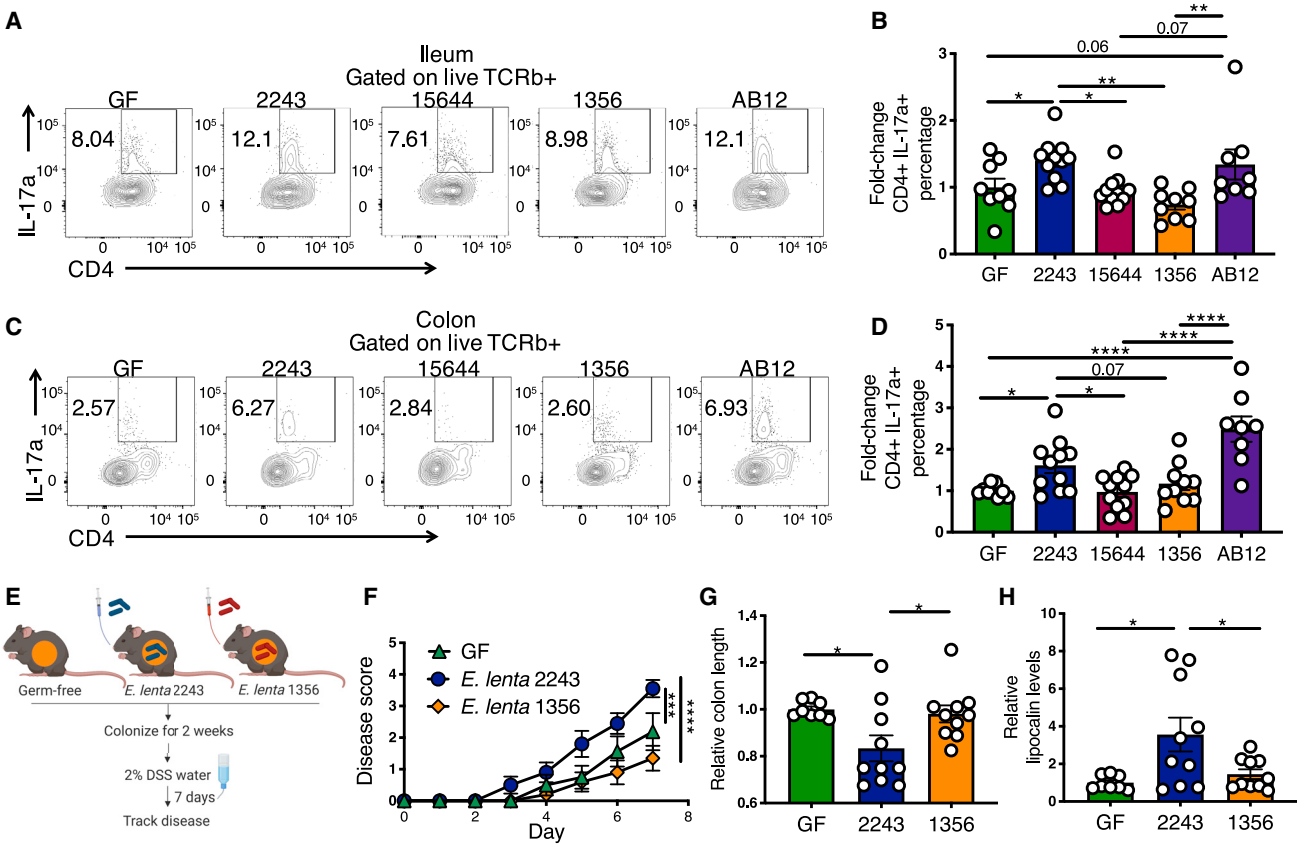

Figure 4. Th17 activation and colitis severity varies between *E. lenta* strains

(A–D) Representative flow plots and fold-change relative to germ-free (GF) of the IL-17a$^+$ CD4$^+$ within the live TCRβ^+ gate in the (A and B) ileal and (C and D) colonic lamina propria from GF mice or *E. lenta* 2243, 15644, 1356, or AB12 monocolonized mice. Data from 2 independent experiments (n = 8–11).

(E–H) GF mice or mice monocolonized with *E. lenta* 2243 or 1356 for 2 weeks were treated with 2% DSS and (F) disease was tracked for 7 days (n = 8–10). p values are two-way ANOVA with Sidak test. (G) Day 7 colon lengths. (H) Lipocalin levels as quantified via ELISA in the colon content. (G and H) are relative to GF.

*p < 0.05; **p < 0.01, ***p < 0.001; ****p < 0.0001; listed; one-way ANOVA with Holm Sidak or Tukey test unless otherwise noted.

Mean ± SEM is displayed. Each dot represents an individual mouse. Model figures made with BioRender.com. See also Figures S2 and S5 and Data S1 and S2.

thiostrepton inducer. CFS from *R. erythropolis* with induced *cgr2*:*WT* expression resulted in a significant increase in Th17 cells compared with uninduced or BHI controls (Figures 5D and S6F–S5H). The partial loss-of-function mutant *cgr2*:Y333N had an intermediate phenotype where Th17 levels were increased when expression was induced compared with uninduced but to a lesser degree than for *cgr2*:*WT* (Figures 5D and S6F–S6H). These findings demonstrate that the gut bacterial enzyme, Cgr2, is sufficient to increase Th17 activation *in vivo*.

The *cgr2* gene correlates with IBD severity and is elevated in subjects with rheumatoid arthritis

Due to our finding that *cgr2* is sufficient to induce Th17 cells, we postulated that *cgr2* may be associated with Th17-driven diseases such as RA and IBD. In a deposited IBD dataset (Franzosa et al., 2019), prevalence of *cgr2* trended higher in subjects with ulcerative colitis or Crohn's disease compared with controls (Figure 5E). We were also interested to see if *cgr2*+ *E. lenta* were associated with IBD disease severity. In stool samples from 18 ulcerative colitis subjects, *E. lenta* levels were significantly correlated with disease scores when *cgr2* was detected; however, there was no significant association when *cgr2* was undetected (Figure 5F). Within *cgr2*+ samples, the proportion of *cgr2*+ *E. lenta* strains ranged from 60%-100% (Figure 5G). We were also interested in determining if *cgr2* levels were altered in another autoimmune disease such as RA. *Cgr2* levels were significantly higher in RA patient stool compared with controls (Figure 5H). 83% of the RA patient samples had detectable *cgr2* compared with 54% in controls (Figure 5I). These results provide initial support for the translational relevance of this specific bacterial gene in human autoimmunity.

Characterization of Th17-modulatory factors metabolized by *cgr2*+ *E. lenta*

Our findings indicate that Cgr2 mediates *E. lenta*-Th17 activation; however, the known Cgr2 substrates are unique to pharmaceuticals and toxic plants (Koppel et al., 2018) and should not be present in these experiments. Therefore, we sought to identify additional Th17-modulatory Cgr2 substrates. We fractionated 3 kDa filtered BHI media, *cgr2*+ *E. lenta* 2243, and *cgr2*− 1356 CFS using reverse phase high performance liquid chromatography (RP-HPLC), then tested IL-17a induction in our Th17 assay (Figure 6A).

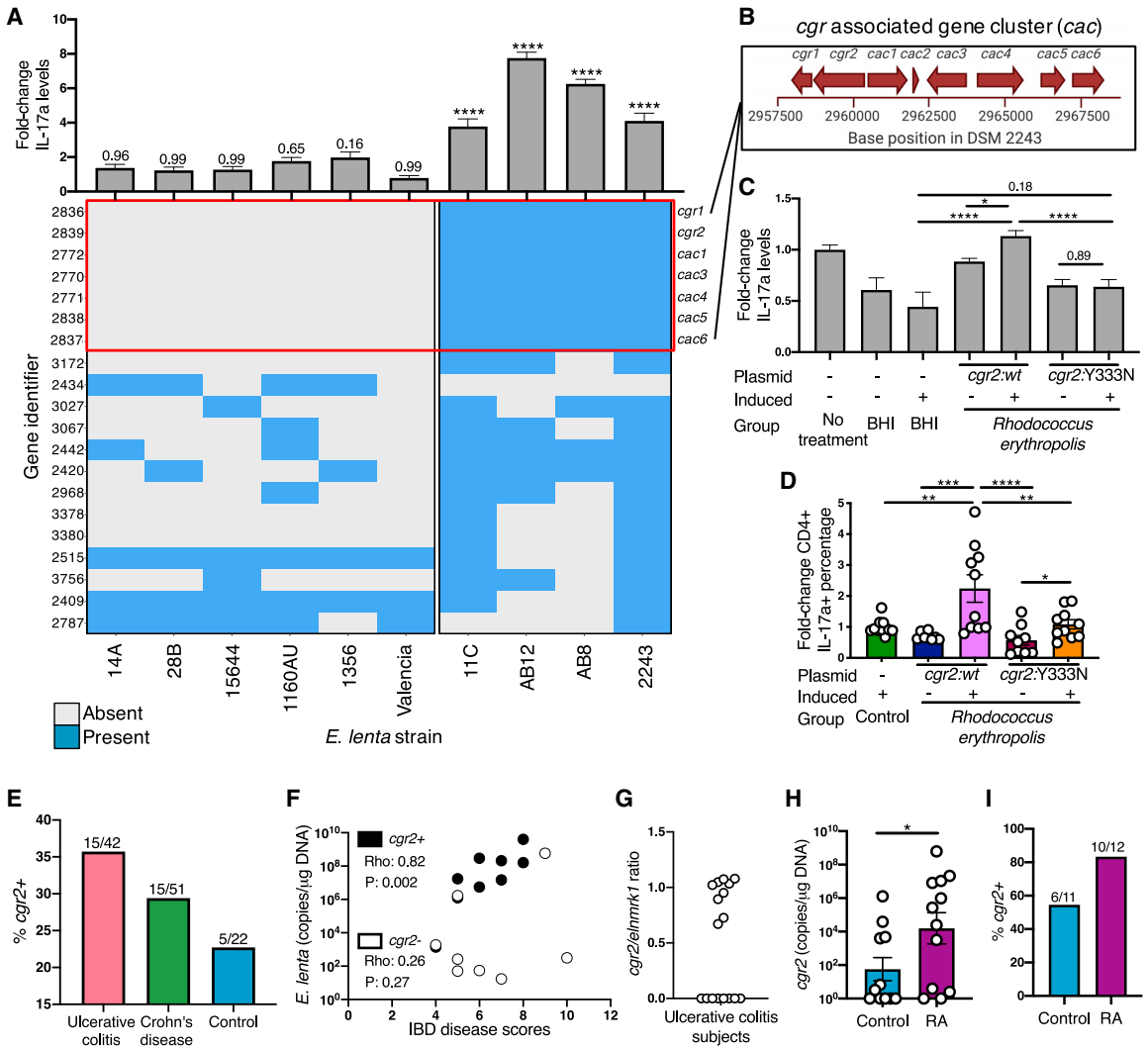

Figure 5. The gut bacterial enzyme Cgr2 is associated with and sufficient for IL-17a induction and associated with autoimmune disease states

(A) Th17 skewed CD4$^+$ T cells were treated with CFS from *E. lenta* strains (14A, 28B, 15644, 1160AU, 1356, Valencia, 11C, AB12, AB8, 2243), or a BHI media control. Fold-change in IL-17a levels (relative to BHI) as measured via ELISA. *E. lenta* strains were classified as not significantly different from BHI ($p > 0.05$) or significantly higher than BHI ($p < 0.05$) by a one-way ANOVA Dunnett's test (listed above each bar). With these classifications we performed comparative genomics using ElenMatchR (Bisanz et al., 2020) (n = 8–12).

(B) Genes in the red box correspond to the cardiac glycoside reductase (*cgr*)-associated gene cluster (*cac*) (Koppel et al., 2018).

(C) Fold-change of IL-17a relative to no treatment in Th17 skewed cells treated with *Rhodococcus erythropolis* CFS with induced (+thiostrepton) or uninduced (−thiostrepton) expression of *cgr2*:*WT* (n = 14), a partial loss-of-function variant *cgr2*:Y333N (n = 12), no treatment (n = 14), or BHI (n = 8–12). p values are one-way ANOVA with Holm Sidak test.

(D) C57BL/6J SPF mice were gavaged with CFS from *R. erythropolis* with induced or uninduced expression of *cgr2*:*WT*, *cgr2*:Y333N, or a BHI+thiostrepton. Fold-change of CD4$^+$ IL-17a$^+$ cells within the live CD3$^+$ gate in the ileal lamina propria relative to BHI (n = 10). Data represent a combination of at least two independent experiments for (A–D). p values are one-way ANOVA with Tukey test.

(E) Shotgun metagenomic analysis from the PRISM IBD study (Franzosa et al., 2019). *cgr2* presence was determined when $\geq$ 0.35 gene copies per cell were present within an *E. lenta*+ sample. Crohn's disease (n = 68), ulcerative colitis (n = 53), and controls (n = 34). A chi-squared test of independence determined no significant differences in *cgr2* carriage.

(F) The correlation of Mayo Clinic disease activity scoring with *cgr2*+ *E. lenta* (black n = 9) or *cgr2*− *E. lenta* (white n = 8) levels in *E. lenta*+ samples from ulcerative colitis stool samples. Rho values, p values are one-tailed Pearson correlations.

(G) Ratio of *cgr2* to the universal *E. lenta* marker *elnmrk1* in the same ulcerative colitis subjects in (F).

(H) *cgr2* copies/µg DNA in healthy (n = 11) and rheumatoid arthritis (RA) (n = 12) stool samples. p values are Mann-Whitney.

(I) *cgr2* prevalence in healthy and RA stool samples with the number of positive samples over total sample numbers on top of bars. p = 0.15, one-sided Fisher's exact test.

*p < 0.05; **p < 0.01; ***p < 0.001; ****p < 0.0001; listed.

Mean ± SEM is displayed. Each point represents an individual subject. See also Figures S2 and S5 and Data S3.

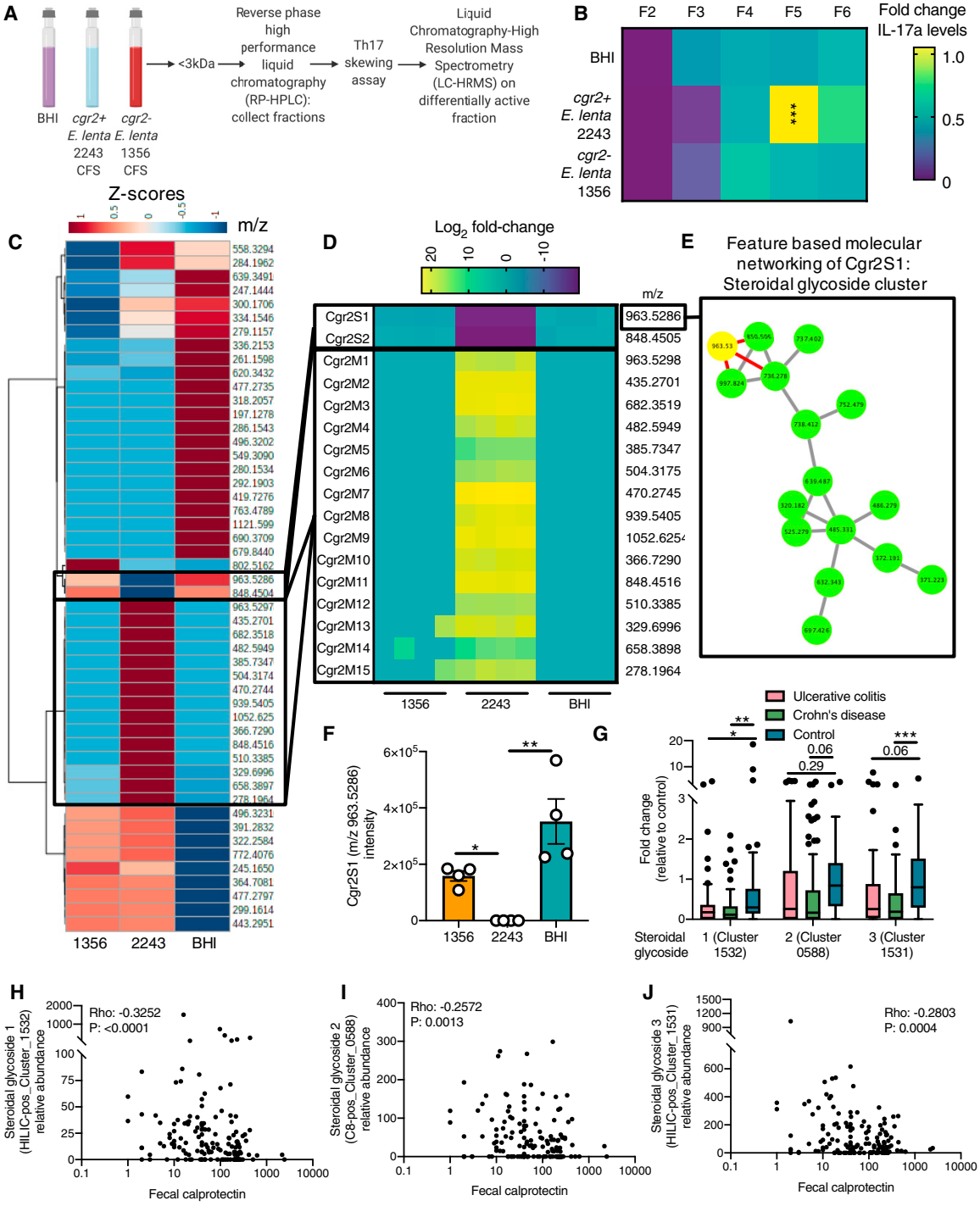

Figure 6. Characterization of Th17-modulatory factors metabolized by *cgr2+ E. lenta*

(A and B) BHI media control, *cgr2+ E. lenta* 2243, and *cgr2-* 1356 3 kDa filtered cell-free supernatant (CFS) were fractionated using RP-HPLC for our Th17 assay. Differentially active fractions were analyzed with LCHRMS. (B) RP-HPLC fractions 2–6 from BHI, 2243, and 1356 CFS were administered to Th17 skewed cells. Fold-change in IL-17a levels (relative to no treatment) was assessed via ELISA. p value is a one-way ANOVA with Holm Sidak's test.

(C and D) LCHRMS was performed on RP-HPLC fraction 5 from BHI, 2243, and 1356 CFS. Top 50 differentially abundant features (by p value, one-way ANOVA) Z scores displayed in a hierarchical clustered heatmap. (D) Log_2 fold-change of putative Cgr2 substrates (Cgr2S1-2) and putative Cgr2 metabolites (Cgr2M1-15) (n = 4/group).

(E) Feature-based molecular networking analysis of Cgr2S1 - m/z 963.5286 (yellow), which is in the lipids/lipid-like molecules, steroidal glycoside cluster (cosine score of 0.3889 for steroidal glycoside parent class assignment for Cgr2S1).

(F) Intensity values of Cgr2S1 - m/z 963.5286 from LCHRMS analysis of RP-HPLC fraction 5. p values are one-way ANOVA with Holm Sidak tests.

(legend continued on next page)

Differential IL-17a induction was seen in fraction 5, suggesting that a nonpolar small molecule was responsible (Figure 6B). To identify potential Cgr2 substrates (Cgr2S), we performed liquid chromatography high-resolution mass spectrometry (LCHRMS) on fraction 5. We found two *m/z*, 963.5286 (Cgr2S1) and 848.4505 (Cgr2S2), that were significantly higher in BHI and 1356 than 2243, fitting the expected pattern of a Cgr2 substrate (Figures 6C and 6D; Data S4). To identify potential Cgr2 metabolites (Cgr2M), we investigated if compounds present in 2243 were absent in BHI and 1356 (Figures 6C and 6D). Due to the reductase capabilities of Cgr2 (Haiser et al., 2013; Koppel et al., 2018), we investigated the m/z unique to 2243 where a shift of 2 consistent with a reduction event; however, no features were identified that fit this pattern for either substrate.

Next, we used feature-based molecular networking analysis (FBMN) (Nothias et al., 2020) to annotate putative Cgr2 substrates. Cgr2S1 was predicted to be a steroidal glycoside (sterol lipids with a carbohydrate moiety glycosidically linked to a steroid skeleton) (Figure 6E) that had significantly higher intensities in BHI and 1356 compared with 2243 (Figure 6F). Cgr2S2 remained unannotated. Cgr2 metabolizes the chemically similar cardiac glycosides and cardenolides (Haiser et al., 2013; Koppel et al., 2018), including the Th17-inhibitory digoxin, into a less potent inhibitor (Huh and Littman, 2012). Taken together, these results support the hypothesis that *cgr2*+ *E. lenta* metabolize endogenous Th17-inhibitory steroidal glycosides into less potent inhibitors resulting in Th17 activation and worsened colitis. More work is necessary to fully purify and solve the structure of each of these putative Cgr2 substrates and metabolites, enabling more controlled studies of Th17 activation.

While our findings indicate that Cgr2 metabolizes Th17-inhibitory steroidal glycosides present in culture media; the translational relevance of these compounds for human autoimmunity remains unclear. To begin to address this question, we used metabolomic datasets from the prospective registry in IBD study at MGH (PRISM) (Franzosa et al., 2019). Of the 7 annotated steroidal glycosides, 3 were significantly depleted in IBD states and/or negatively correlated with fecal calprotectin levels (Figures 6G–6J). While we did not find an exact match to the m/z of the Cgr2S1 or Cgr2S2, these findings indicate that steroidal glycosides are present in humans, differentially abundant in disease states, and negatively correlated with disease severity metrics, making steroidal glycosides and exciting area of future investigations for their importance to human disease.

Dietary arginine inhibits Th17 activation and colitis induction by *cgr2*+ *E. lenta*

Given the clinical relevance of *E. lenta* and *cgr2* across multiple autoimmune diseases, we sought to identify a non-invasive strategy for blocking this metabolic activity without profoundly disrupting the gut microbiome. We leveraged prior data demonstrating that dietary protein intake, likely due to the increased arginine (Arg) levels in the gut lumen, blocks Cgr2 reduction of the cardiac drug digoxin (Haiser et al., 2013). We hypothesized that elevated Arg would have a similar ability to prevent *cgr2*+ *E. lenta* mediated Th17 activation and associated disease phenotypes.

We designed two matched diets differing in Arg levels: 1% or 3% per kg (Table S2). GF mice were fed the 1% or 3% Arg diets for 3 days prior to colonization with *cgr2*+ *E. lenta* 2243 or *cgr2*− 15644 for 2 weeks (Figure 7A; Table S2). 2243 colonized mice had significantly increased Th17 cells on the 1% Arg diet compared with GF or mice colonized with 15644 (Figures 7B and 7C), as expected based on *cgr2* status. Consumption of the 3% Arg diet rescued this effect, significantly decreasing Th17 levels in 2243 colonized mice (Figures 7B and 7C). *E. lenta* colonization levels did not differ between the diets (Figure S7A), suggesting that the differences in immune function are driven by diet-dependent changes in bacterial metabolism independent of colonization efficiency.

Finally, we tested if dietary Arg could rescue the impact of *E. lenta* on colitis severity. We gavaged *cgr2*+ *E. lenta* 2243 or *cgr2*− 15644 into SPF mice on a 1% or 3% Arg diet for 2 weeks and then induced DSS colitis (Figure 7D). Th17 cell levels were consistent with our prior experiment (Figures S7B and S7C) and the only group with elevated severity was *cgr2*+ 2243 on a 1% Arg diet (Figures 7E–7G), emphasizing the importance of both dietary context and strain-level variation for determining host immunological and disease phenotypes.

DISCUSSION

Our results provide evidence for a role of the prevalent human gut Actinobacterium, *E. lenta*, across numerous autoimmune diseases. Historically, studies on *E. lenta* focused on its role in bacteremia (Gardiner et al., 2015), but more recently *E. lenta* has been associated with MS and RA (Cekanaviciute et al., 2017; Zhang et al., 2015). Our results show that *E. lenta* is also enriched in IBD patients and worsens models of colitis. Further, we identified a gene cluster, *cac*, that is necessary and a specific gene within this cluster, *cgr2,* that is sufficient for Th17 activation in mice and associated with disease in humans. The broad relevance of *E. lenta* and *cgr2* in autoimmunity is supported by a recently published study on two additional autoimmune diseases where *cgr2*+ *E. lenta* were enriched in disease states (Plichta et al., 2021).

The potential for broad impacts of *E. lenta* across diverse disease states is increased due to the effect of this gut bacterium on Th17 cells coupled to the lack of antigen specificity. Our findings differ from prior work on bacteria and fungi, which are thought to involve specific antigens and/or require epithelial adhesion (Atarashi et al., 2015; Bacher et al., 2019). In contrast, *E. lenta* can act on Th17 cells post-differentiation and at a distance. These findings raise the potential for effects on Th17 cells in other tissues outside the gut or for synergistic effects with previously described antigen-specific responses.

(G) Steroidal glycosides (1: HILIC-pos_Cluster_1532, 2: C8-pos_Cluster_0588, 3: HILIC-pos_Cluster_1531) fold-change relative to controls in the PRISM and NLIBD/LLDeep IBD studies (Franzosa et al., 2019). Crohn's disease (n = 88), ulcerative colitis (n = 76), and controls (n = 56).

(H–J) Correlation of steroidal glycosides relative abundance from the PRISM and NLIBD/LLDeep IBD studies to fecal calprotectin levels (μg/g). Spearman rho, p values listed.

*p < 0.05; **p < 0.01; ***p < 0.001; ****p < 0.0001; listed.

Data are displayed as heatmaps, Tukey box and whisker plots, individual points, or as mean ± SEM. Model figures made with BioRender.com. See also Data S4.

CellPress
OPEN ACCESS

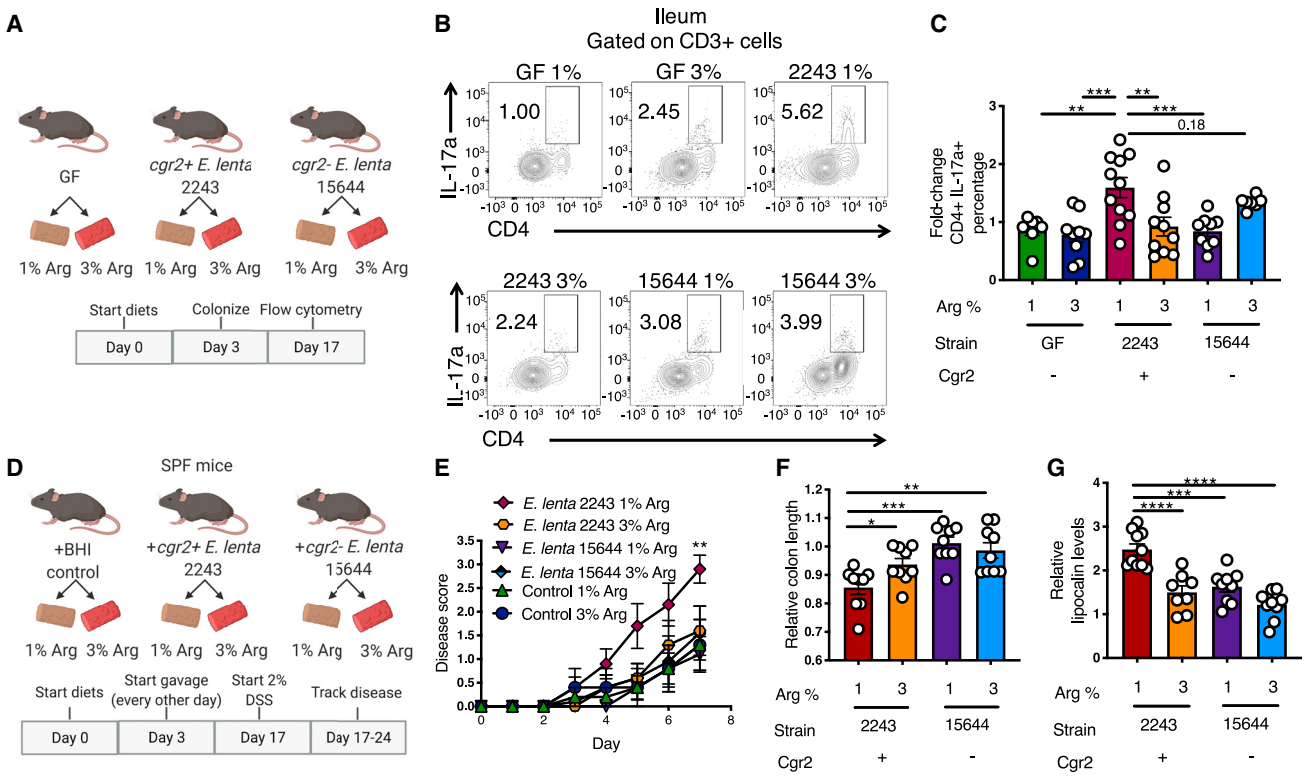

Figure 7. Dietary arginine inhibits Th17 activation and colitis induction by *cgr2+ E. lenta*

(A–C) Analysis of Th17 cells in germ-free (GF), *E. lenta* 2243, or 15644 monocolonized mice on a 1% or 3% arginine (Arg) diet. (B) Representative flow plots and (C) fold-change of $CD4^+$ IL-$17a^+$ cells within the live $CD3^+$ in the ileal lamina propria relative to the GF 1% Arg. Data are from 2 independent experiments (n = 8–11). (D–G) SPF mice on a 1% or 3% Arg diet were gavaged with BHI, 2243, or 15644 for 2 weeks then treated with 2% DSS. (E) Disease scores over 7 days. p values are two-way ANOVA with Sidak test (1% versus 3% 2243) (n = 5–10). (F) Relative colon lengths. (G) Relative lipocalin in colon content. Levels are relative to the BHI control diet in (F and G). Data are from 2 independent experiments.

*p < 0.05; **p < 0.01; ***p < 0.001; ****p < 0.0001 one-way ANOVA with Tukey test unless otherwise stated. Mean ± SEM is displayed. Each point represents an individual mouse. Model figures made with BioRender.com. See also Figures S2 and S7.

Our work also suggests that further investigations are warranted to study immunomodulatory effects of endogenous steroidal glycosides and the full extent of their metabolism by host and microbial enzymes. Prior studies demonstrated that the cardiac glycoside digoxin inhibits Rorγt, decreasing severity of models of autoimmunity (Fujita-Sato et al., 2011; Huh et al., 2011). Our work suggests that steroidal glycosides present in bacterial culture media are metabolized by the Cgr2 enzyme of *E. lenta* leading to downstream effects on immune activation. Yet, more work is needed to purify and solve the structures of the putative Cgr2 substrates and metabolites identified herein, enabling in-depth biochemical, immunological, and microbiological characterizations. It will also be important to identify the source(s) of these compounds and the factors that control their concentration in mice and humans.

Diet is a key regulator of the microbiota and microbial-mediated immune modulation. Our findings suggest that dietary Arg levels could be used to tune Th17 activity in *cgr2+ E. lenta* colonized subjects. The potential off-target effects of dietary Arg due to its *E. lenta*-independent immunomodulatory activities (Coburn et al., 2012; O'Neill et al., 2016) could complicate the goal of using diet to tune immune responses in a beneficial manner. Despite this, multiple observations support a general beneficial effect of Arg for IBD. Subjects with IBD have a significant negative correlation between colonic tissue Arg levels and disease activity indexes (Coburn et al., 2016) and Arg supplementation improved DSS colitis outcomes (Ren et al., 2014; Singh et al., 2019). Together with previous work, our study expands on the general mechanisms by which diet alters microbial-derived immunomodulatory metabolites demonstrating the feasibility of altering microbial immunomodulation with diet.

While our findings provide a compelling link between select strains of *E. lenta* and disease, more work is needed to place these observations in the broader context of the full metabolic capabilities of this bacterial species, let alone the rest of the gut microbiota. Our collaborators have shown that *E. lenta* can produce metabolites with opposing effects on Th17 activation such as 3-oxo-lithocholic acid (LCA) and isoLCA via bile acid hydroxysteroid dehydrogenases (Paik et al., 2021). These results, together with the current study, emphasize the potential for the metabolic capabilities of a single bacterial strain (e.g., DSM 2243) to both activate and inhibit Th17 cells. The balance between these mechanisms requires more sophisticated models and would likely involve interactions with other bacteria necessary for bile acid metabolism.

In conclusion, these results expand the mechanisms through which bacteria shape mucosal immunity, providing support for a role of human gut bacterial metabolism in driving autoimmunity. Further work is warranted to characterize the range of Th17-modulatory Cgr2 substrates, their structures, and the direct impact of microbial metabolism of specific immunomodulatory compounds on disease. Another important future direction of this work will be examining if modulation of *E. lenta* levels and/or metabolic activity in humans with antibiotic targeting *E. lenta* or dietary alterations to *E. lenta* metabolism has functional consequences for autoimmune patients.

STAR★METHODS

Detailed methods are provided in the online version of this paper and include the following:

- KEY RESOURCES TABLE
- RESOURCE AVAILABILITY
  - Lead contact
  - Materials availability
  - Data and code availability
- EXPERIMENTAL MODEL AND SUBJECT DETAILS
  - Experimental design
  - Mice
  - Gnotobiotic mouse studies
  - SPF mouse studies
  - DSS disease model
  - *IL-10-/-* colitis model
  - Diets
  - Human subjects
  - Inflammatory bowel disease (ulcerative colitis) patient fecal samples
- METHOD DETAILS
  - Bacterial culturing
  - Heterologous expression
  - Th17 skewing assay
  - Rorγ luciferase assay
  - Antigen specificity experiments
  - ELISAs
  - Lamina propria lymphocyte isolation
  - Flow cytometry
  - Histology
  - *E. lenta* comparative genomics
  - RNA/DNA isolation and qPCR
  - RNA sequencing
  - RP-HPLC
  - LCHRMS and analysis
  - Metagenomic data analysis
- QUANTIFICATION AND STATISTICAL ANALYSIS

SUPPLEMENTAL INFORMATION

Supplemental information can be found online at https://doi.org/10.1016/j.chom.2021.11.001.

ACKNOWLEDGMENTS

We acknowledge: UCSF Gnotobiotics Core (gnotobiotics.ucsf.edu); Baron lab (*Rorc*$^{-/-}$ mice); Balskus lab (*R. erythropolis*, *cgr2*:*WT*, *Y333N*); Chunyu Zhao (metagenomic intra-species diversity analysis subcommands [MIDAS]/IGGtools); PFCC (P30DK063720); BTBT (histology); IHG core (RNA-seq); and UCSF QMAC (metabolomics). We thank Janice Goh for help with RNA-seq and Kathy Lam, Tiffany Scharschmidt, Rachel Rock and Mark Ansel for critical feedback. Funding: NIH (R01HL122593, R21CA227232, R01AR074500, R01DK114034 (P.J.T.); 5T32AI060537, F32AI14745601 (M.A.); 5T32 AR00730437, TR001871, K08AR073930 (R.N.); 5T32DK00700745 (B.Z.); T32HL007185 (V.U)), Searle Scholars Program (SSP20161352), MedImmune, Gladstone Institutes, the Breakthrough Program for Rheumatoid-related Arthritis Research, and a PhRMA Fellowship (A.E.B.). K.S.P. is a Chan Zuckerberg Biohub PI. P.J.T. was a Nadia's Gift Foundation Innovator supported, in part, by the Damon Runyon Cancer Research Foundation (DRR4216).

AUTHOR CONTRIBUTIONS

Conceptualization, M.A. and P.J.T.; investigation, M.A., Q.A., R.N., V.U., M.S., A.E.B., and B.Z.; resources, P.J.T. and S.V.L.; writing – original draft, M.A; writing – review & editing, M.A., Q.Y.A., R.N., M.S., V.U., P.J.T., K.S.P., B.Z., and S.V.L.; supervision, P.J.T., K.S.P., and S.V.L.

DECLARATION OF INTERESTS

P.J.T. is on the scientific advisory board for Kaleido, Pendulum, and SNIPRbiome. K.S.P. is on the scientific advisory board of Phylagen. S.V.L. is a cofounder, board member, and consultant for Siolta Therapeutics Inc. This work was partially supported by a MedImmune research grant.

INCLUSION AND DIVERSITY

We worked to ensure gender balance in the recruitment of human subjects, ethnic or other types of diversity in the recruitment of human subjects, that the study questionnaires were prepared in an inclusive way, and sex balance in the selection of non-human subjects. One or more of the authors of this paper received support from a program designed to increase minority representation in science. While citing references scientifically relevant for this work, we also actively worked to promote gender balance in our reference list.

Received: November 17, 2020
Revised: October 21, 2021
Accepted: November 3, 2021
Published: November 24, 2021

REFERENCES

Aletaha, D., Neogi, T., Silman, A.J., Funovits, J., Felson, D.T., Bingham, C.O., 3rd, Birnbaum, N.S., Burmester, G.R., Bykerk, V.P., Cohen, M.D., et al. (2010). 2010 rheumatoid arthritis classification criteria: an American College of Rheumatology/European League Against Rheumatism collaborative initiative. Arthritis Rheum. *62*, 2569–2581.

Alexander, M., and Turnbaugh, P.J. (2020). Deconstructing mechanisms of diet-microbiome-immune interactions. Immunity *53*, 264–276.

Almeida, A., Nayfach, S., Boland, M., Strozzi, F., Beracochea, M., Shi, Z.J., Pollard, K.S., Parks, D.H., Hugenholtz, P., Segata, N., et al. (2019). A unified sequence catalogue of over 280,000 genomes obtained from the human gut microbiome. bioRxiv, 32690973. https://www.biorxiv.org/content/10.1101/762682v1.full.pdf.

Ang, Q.Y., Alexander, M., Newman, J.C., Tian, Y., Cai, J., Upadhyay, V., Turnbaugh, J.A., Verdin, E., Hall, K.D., Leibel, R.L., et al. (2020). Ketogenic diets alter the gut microbiome resulting in decreased intestinal Th17 cells. Cell *181*, 1263–1275.e16.

Atarashi, K., Tanoue, T., Ando, M., Kamada, N., Nagano, Y., Narushima, S., Suda, W., Imaoka, A., Setoyama, H., Nagamori, T., et al. (2015). Th17 cell induction by adhesion of microbes to intestinal epithelial cells. Cell *163*, 367–380.

Atarashi, K., Tanoue, T., Shima, T., Imaoka, A., Kuwahara, T., Momose, Y., Cheng, G., Yamasaki, S., Saito, T., Ohba, Y., et al. (2011). Induction of colonic regulatory T cells by indigenous Clostridium species. Science *331*, 337–341.

Bacher, P., Hohnstein, T., Beerbaum, E., Röcker, M., Blango, M.G., Kaufmann, S., Röhmel, J., Eschenhagen, P., Grehn, C., Seidel, K., et al. (2019). Human anti-fungal Th17 immunity and pathology rely on cross-reactivity against Candida albicans. Cell *176*, 1340–1355.e15.

Belkaid, Y., and Hand, T.W. (2014). Role of the microbiota in immunity and inflammation. Cell *157*, 121–141.

Bisanz, J.E., Soto-Perez, P., Noecker, C., Aksenov, A.A., Lam, K.N., Kenney, G.E., Bess, E.N., Haiser, H.J., Kyaw, T.S., Yu, F.B., et al. (2020). A genomic toolkit for the mechanistic dissection of intractable human gut bacteria. Cell Host Microbe *27*, 1001–1013.e9.

Britton, G.J., Contijoch, E.J., Mogno, I., Vennaro, O.H., Llewellyn, S.R., Ng, R., Li, Z., Mortha, A., Merad, M., Das, A., et al. (2019). Microbiotas from humans with inflammatory bowel disease alter the balance of gut Th17 and RORγt+ regulatory T cells and exacerbate colitis in mice. Immunity *50*, 212–224.e4.

Britton, G.J., Contijoch, E.J., Spindler, M.P., Aggarwala, V., Dogan, B., Bongers, G., San Mateo, L., Baltus, A., Das, A., Gevers, D., et al. (2020). Defined microbiota transplant restores Th17/RORγt+ regulatory T cell balance in mice colonized with inflammatory bowel disease microbiotas. Proc. Natl. Acad. Sci. USA *117*, 21536–21545.

Cekanaviciute, E., Yoo, B.B., Runia, T.F., Debelius, J.W., Singh, S., Nelson, C.A., Kanner, R., Bencosme, Y., Lee, Y.K., Hauser, S.L., et al. (2017). Gut bacteria from multiple sclerosis patients modulate human T cells and exacerbate symptoms in mouse models. Proc. Natl. Acad. Sci. USA *114*, 10713–10718.

Chassaing, B., Aitken, J.D., Malleshappa, M., and Vijay-Kumar, M. (2014). Dextran sulfate sodium (DSS)-induced colitis in mice. Curr. Protoc. Immunol. *104*, 15.25.1–15.25.14.

Chen, Y., Ye, W., Zhang, Y., and Xu, Y. (2015). High speed BLASTn: an accelerated MegaBLAST search tool. Nucleic Acids Res. *43*, 7762–7768.

Ciofani, M., Madar, A., Galan, C., Sellars, M., Mace, K., Pauli, F., Agarwal, A., Huang, W., Parkhurst, C.N., Muratet, M., et al. (2012). A validated regulatory network for Th17 cell specification. Cell *151*, 289–303.

Coburn, L.A., Gong, X., Singh, K., Asim, M., Scull, B.P., Allaman, M.M., Williams, C.S., Rosen, M.J., Washington, M.K., Barry, D.P., et al. (2012). L-arginine supplementation improves responses to injury and inflammation in dextran sulfate sodium colitis. PLoS One *7*, e33546.

Coburn, L.A., Horst, S.N., Allaman, M.M., Brown, C.T., Williams, C.S., Hodges, M.E., Druce, J.P., Beaulieu, D.B., Schwartz, D.A., and Wilson, K.T. (2016). L-arginine availability and metabolism is altered in ulcerative colitis. Inflamm. Bowel Dis. *22*, 1847–1858.

da Silva, R.R., Wang, M., Nothias, L.F., van der Hooft, J.J.J., Caraballo-Rodríguez, A.M., Fox, E., Balunas, M.J., Klassen, J.L., Lopes, N.P., and Dorrestein, P.C. (2018). Propagating annotations of molecular networks using in silico fragmentation. PLoS Comput. Biol. *14*, e1006089.

Dumas, A., Corral, D., Colom, A., and Levillain, F. (2018). The host microbiota contributes to early protection against lung colonization by Mycobacterium tuberculosis. Front Immunol *9*, 2656.

Ernst, M., Kang, K.B., Caraballo-Rodríguez, A.M., Nothias, L.F., Wandy, J., Chen, C., Wang, M., Rogers, S., Medema, M.H., Dorrestein, P.C., and van der Hooft, J.J.J. (2019). MolNetEnhancer: enhanced molecular networks by integrating metabolome mining and annotation tools. Metabolites *9*, 144.

Fernandes, A.D., Macklaim, J.M., Linn, T.G., Reid, G., and Gloor, G.B. (2013). ANOVA-like differential expression (ALDEx) analysis for mixed population RNA-seq. PLoS One *8*, e67019.

Fernandes, A.D., Reid, J.N., Macklaim, J.M., McMurrough, T.A., Edgell, D.R., and Gloor, G.B. (2014). Unifying the analysis of high-throughput sequencing datasets: characterizing RNA-seq, 16S rRNA gene sequencing and selective growth experiments by compositional data analysis. Microbiome *2*, 15.

Frank, D.N., St Amand, A.L., Feldman, R.A., Boedeker, E.C., Harpaz, N., and Pace, N.R. (2007). Molecular-phylogenetic characterization of microbial community imbalances in human inflammatory bowel diseases. Proc. Natl. Acad. Sci. USA *104*, 13780–13785.

Franzosa, E.A., Sirota-Madi, A., Avila-Pacheco, J., Fornelos, N., Haiser, H.J., Reinker, S., Vatanen, T., Hall, A.B., Mallick, H., McIver, L.J., et al. (2019). Gut microbiome structure and metabolic activity in inflammatory bowel disease. Nat. Microbiol. *4*, 293–305.

Fujita-Sato, S., Ito, S., Isobe, T., Ohyama, T., Wakabayashi, K., Morishita, K., Ando, O., and Isono, F. (2011). Structural basis of digoxin that antagonizes RORγt receptor activity and suppresses Th17 cell differentiation and interleukin (IL)-17 production. J. Biol. Chem. *286*, 31409–31417.

Gardiner, B.J., Tai, A.Y., Kotsanas, D., Francis, M.J., Roberts, S.A., Ballard, S.A., Junckerstorff, R.K., and Korman, T.M. (2015). Clinical and microbiological characteristics of Eggerthella lenta bacteremia. J. Clin. Microbiol. *53*, 626–635.

Geng, J., Wei, H., Shi, B., Wang, Y.H., Greer, B.D., Pittman, M., Smith, E., Thomas, P.G., Kutsch, O., and Hu, H. (2019). Bach2 negatively regulates T follicular helper cell differentiation and is critical for CD4+ T cell memory. J. Immunol. *202*, 2991–2998.

Gloor, G.B., Macklaim, J.M., Pawlowsky-Glahn, V., and Egozcue, J.J. (2017). Microbiome datasets are compositional: and this is not optional. Front. Microbiol. *8*, 2224.

Goto, Y., Panea, C., Nakato, G., Cebula, A., Lee, C., Diez, M.G., Laufer, T.M., Ignatowicz, L., and Ivanov, I.I. (2014). Segmented filamentous bacteria antigens presented by intestinal dendritic cells drive mucosal Th17 cell differentiation. Immunity *40*, 594–607.

Guo, Y., MacIsaac, K.D., Chen, Y., Miller, R.J., Jain, R., Joyce-Shaikh, B., Ferguson, H., Wang, I.M., Cristescu, R., Mudgett, J., et al. (2016). Inhibition of RORγT skews TCRα gene rearrangement and limits T cell repertoire diversity. Cell Rep *17*, 3206–3218.

Haiser, H.J., Gootenberg, D.B., Chatman, K., Sirasani, G., Balskus, E.P., and Turnbaugh, P.J. (2013). Predicting and manipulating cardiac drug inactivation by the human gut bacterium Eggerthella lenta. Science *341*, 295–298.

He, Y.W., Deftos, M.L., Ojala, E.W., and Bevan, M.J. (1998). RORγt, a novel isoform of an orphan receptor, negatively regulates Fas ligand expression and IL-2 production in T cells. Immunity *9*, 797–806.

Hu, R., Kagele, D.A., Huffaker, T.B., Runtsch, M.C., Alexander, M., Liu, J., Bake, E., Su, W., Williams, M.A., Rao, D.S., et al. (2014). miR-155 promotes T follicular helper cell accumulation during chronic, low-grade inflammation. Immunity *41*, 605–619.

Huh, J.R., Leung, M.W.L., Huang, P., Ryan, D.A., Krout, M.R., Malapaka, R.R.V., Chow, J., Manel, N., Ciofani, M., Kim, S.V., et al. (2011). Digoxin and its derivatives suppress TH17 cell differentiation by antagonizing RORγt activity. Nature *472*, 486–490.

Huh, J.R., and Littman, D.R. (2012). Small molecule inhibitors of RORγt: targeting Th17 cells and other applications. Eur. J. Immunol. *42*, 2232–2237.

Ivanov, I.I., Atarashi, K., Manel, N., Brodie, E.L., Shima, T., Karaoz, U., Wei, D., Goldfarb, K.C., Santee, C.A., Lynch, S.V., et al. (2009). Induction of intestinal Th17 cells by segmented filamentous bacteria. Cell *139*, 485–498.

Katajamaa, M., Miettinen, J., and Oresic, M. (2006). MZmine: toolbox for processing and visualization of mass spectrometry based molecular profile data. Bioinformatics *22*, 634–636.

Kawashima, M., Kawakita, T., Inaba, T., Okada, N., Ito, M., Shimmura, S., Watanabe, M., Shinmura, K., and Tsubota, K. (2012). Dietary lactoferrin alleviates age-related lacrimal gland dysfunction in mice. PLoS One *7*, e33148.

Koppel, N., Bisanz, J.E., Pandelia, M.E., Turnbaugh, P.J., and Balskus, E.P. (2018). Discovery and characterization of a prevalent human gut bacterial enzyme sufficient for the inactivation of a family of plant toxins. eLife *7*, e33953.

Kubinak, J.L., Petersen, C., Stephens, W.Z., Soto, R., Bake, E., O'Connell, R.M., and Round, J.L. (2015). MyD88 signaling in T cells directs IgA-mediated control of the microbiota to promote health. Cell Host Microbe *17*, 153–163.

Lee, H.S., Choi, E.J., Lee, K.S., Kim, H.R., Na, B.R., Kwon, M.S., Jeong, G.S., Choi, H.G., Choi, E.Y., and Jun, C.D. (2016). Oral administration of p-hydroxycinnamic acid attenuates atopic dermatitis by downregulating Th1 and Th2 cytokine production and keratinocyte activation. PLoS One *11*, e0150952.

Lee, Y.K., Menezes, J.S., Umesaki, Y., and Mazmanian, S.K. (2011). Proinflammatory T-cell responses to gut microbiota promote experimental autoimmune encephalomyelitis. Proc. Natl. Acad. Sci. USA *108* (suppl 1), 4615–4622.

Liu, T., Yang, Q., Cao, Y.J., Yuan, W.M., Lei, A.H., Zhou, P., Zhou, W., Liu, Y.D., Shi, M.-H., Yang, Q., et al. (2019). Cyclooxygenase-1 regulates the development of follicular Th cells via prostaglandin E2. J. Immunol. *203*, 864–872.

Love, M.I., Huber, W., and Anders, S. (2014). Moderated estimation of fold change and dispersion for RNA-seq data with DESeq2. Genome Biol *15*, 550.

Maeda, Y., Kurakawa, T., Umemoto, E., Motooka, D., Ito, Y., Gotoh, K., Hirota, K., Matsushita, M., Furuta, Y., Narazaki, M., et al. (2016). Dysbiosis contributes to arthritis development via activation of autoreactive T cells in the intestine. Arthritis Rheumatol *68*, 2646–2661.

Middleton, M.K., Zukas, A.M., Rubinstein, T., Kinder, M., Wilson, E.H., Zhu, P., Blair, I.A., Hunter, C.A., and Puré, E. (2009). 12/15-lipoxygenase-dependent myeloid production of interleukin-12 is essential for resistance to chronic toxoplasmosis. Infect. Immun. *77*, 5690–5700.

Mohimani, H., Gurevich, A., Shlemov, A., Mikheenko, A., Korobeynikov, A., Cao, L., Shcherbin, E., Nothias, L.F., Dorrestein, P.C., and Pevzner, P.A. (2018). Dereplication of microbial metabolites through database search of mass spectra. Nat. Commun. *9*, 4035.

Moore-Smith, L.D., Isayeva, T., Lee, J.H., Frost, A., and Ponnazhagan, S. (2017). Silencing of TGF-β1 in tumor cells impacts MMP-9 in tumor microenvironment. Sci. Rep. *7*, 8678.

Nayfach, S., Rodriguez-Mueller, B., Garud, N., and Pollard, K.S. (2016). An integrated metagenomics pipeline for strain profiling reveals novel patterns of bacterial transmission and biogeography. Genome Res *26*, 1612–1625.

Nothias, L.F., Petras, D., Schmid, R., Dührkop, K., Rainer, J., Sarvepalli, A., Protsyuk, I., Ernst, M., Tsugawa, H., Fleischauer, M., et al. (2020). Feature-based molecular networking in the GNPS analysis environment. Nat. Methods *17*, 905–908.

O'Neill, L.A.J., Kishton, R.J., and Rathmell, J. (2016). A guide to immunometabolism for immunologists. Nat. Rev. Immunol. *16*, 553–565.

Paik, D., Yao, L., Zhang, Y., Bae, S., D'Agostino, G.D., and Kim, E. (2021). Human gut bacteria produce TH17-modulating bile acid metabolites. bioRxiv https://www.biorxiv.org/content/10.1101/2021.01.08.425913v1.

Pang, Z., Chong, J., Zhou, G., de Lima Morais, D.A., Chang, L., Barrette, M., Gauthier, C., Jacques, P.É., Li, S., and Xia, J. (2021). MetaboAnalyst 5.0: narrowing the gap between raw spectra and functional insights. Nucleic Acids Res. *49*, W388–W396.

Plichta, D.R., Somani, J., Pichaud, M., Wallace, Z.S., Fernandes, A.D., Perugino, C.A., Lähdesmäki, H., Stone, J.H., Vlamakis, H., Chung, D.C., et al. (2021). Congruent microbiome signatures in fibrosis-prone autoimmune diseases: IgG4-related disease and systemic sclerosis. Genome Med. *13*, 35.

Pluskal, T., Castillo, S., Villar-Briones, A., and Oresic, M. (2010). MZmine 2: modular framework for processing, visualizing, and analyzing mass spectrometry-based molecular profile data. BMC Bioinformatics *11*, 395.

Qin, J., Li, R., Raes, J., Arumugam, M., Burgdorf, K.S., Manichanh, C., Nielsen, T., Pons, N., Levenez, F., Yamada, T., et al. (2010). A human gut microbial gene catalogue established by metagenomic sequencing. Nature *464*, 59–65.

Ren, W., Yin, J., Wu, M., Liu, G., Yang, G., Xion, Y., Su, D., Wu, L., Li, T., Chen, S., et al. (2014). Serum amino acids profile and the beneficial effects of L-arginine or L-glutamine supplementation in dextran sulfate sodium colitis. PLoS One *9*, e88335.

Round, J.L., Lee, S.M., Li, J., Tran, G., Jabri, B., Chatila, T.A., and Mazmanian, S.K. (2011). The toll-like receptor 2 pathway establishes colonization by a commensal of the human microbiota. Science *332*, 974–977.

Sands, B.E., Peyrin-Biroulet, L., Loftus, E.V., Jr., Danese, S., Colombel, J.F., Törüner, M., Jonaitis, L., Abhyankar, B., Chen, J., Rogers, R., et al. (2019). Vedolizumab versus adalimumab for moderate-to-severe ulcerative colitis. N. Engl. J. Med. *381*, 1215–1226.

Selvig, D., Piceno, Y., Terdiman, J., Zydek, M., Umetsu, S.E., Balitzer, D., Fadrosh, D., Lynch, K., Lamere, B., Leith, T., et al. (2020). Fecal microbiota transplantation in pouchitis: clinical, endoscopic, histologic, and microbiota results from a pilot study. Dig. Dis. Sci. *65*, 1099–1106.

Shao, T.Y., Ang, W.X.G., Jiang, T.T., Huang, F.S., Andersen, H., Kinder, J.M., Pham, G., Burg, A.R., Ruff, B., Gonzalez, T., et al. (2019). Commensal Candida albicans positively calibrates systemic Th17 immunological responses. Cell Host Microbe *25*, 404–417.e6.

Singh, K., Gobert, A.P., Coburn, L.A., Barry, D.P., Allaman, M., Asim, M., Luis, P.B., Schneider, C., Milne, G.L., Boone, H.H., et al. (2019). Dietary arginine regulates severity of experimental colitis and affects the colonic microbiome. Front. Cell. Infect. Microbiol. *9*, 66.

Szőköl, J., Rucká, L., Šimčíková, M., Halada, P., Nešvera, J., and Pátek, M. (2014). Induction and carbon catabolite repression of phenol degradation genes in Rhodococcus erythropolis and Rhodococcus jostii. Appl. Microbiol. Biotechnol. *98*, 8267–8279.

Tachiiri, A., Imamura, R., Wang, Y., Fukui, M., Umemura, M., and Suda, T. (2003). Genomic structure and inducible expression of the IL-22 receptor α chain in mice. Genes Immun. *4*, 153–159.

Tan, T.G., Sefik, E., Geva-Zatorsky, N., Kua, L., Naskar, D., Teng, F., Pasman, L., Ortiz-Lopez, A., Jupp, R., Wu, H.-J.J., et al. (2016). Identifying species of symbiont bacteria from the human gut that, alone, can induce intestinal Th17 cells in mice. Proc. Natl. Acad. Sci. USA *113*, E8141–E8150.

Ueda, A., Zhou, L., and Stein, P.L. (2012). Fyn promotes Th17 differentiation by regulating the kinetics of RORγt and Foxp3 expression. J. Immunol. *188*, 5247–5256.

Wandy, J., Zhu, Y., van der Hooft, J.J.J., Daly, R., Barrett, M.P., and Rogers, S. (2018). Ms2lda.org: Web-based topic modelling for substructure discovery in mass spectrometry. Bioinformatics *34*, 317–318.

Wang, M., Carver, J.J., Phelan, V.V., Sanchez, L.M., Garg, N., Peng, Y., Nguyen, D.D., Watrous, J., Kapono, C.A., Luzzatto-Knaan, T., et al. (2016). Sharing and community curation of mass spectrometry data with Global Natural Products Social Molecular Networking. Nat. Biotechnol. *34*, 828–837.

Wei, B., Zhang, R., Zhai, J., Zhu, J., Yang, F., Yue, D., Liu, X., Lu, C., and Sun, X. (2018). Suppression of Th17 cell response in the alleviation of dextran sulfate sodium-induced colitis by Ganoderma lucidum polysaccharides. J. Immunol. Res. *2018*, 2906494.

Weng, Y.J., Gan, H.Y., Li, X., Huang, Y., Li, Z.C., Deng, H.M., Chen, S.Z., Zhou, Y., Wang, L.S., Han, Y.P., et al. (2019). Correlation of diet, microbiota and metabolite networks in inflammatory bowel disease. J. Dig. Dis. *20*, 447–459.

Yang, J., and Xu, L. (2016). Elevated IL-23R expression and Foxp3+ Rorgt+ cells in intestinal mucosa during acute and chronic colitis. Med. Sci. Monit. *22*, 2785–2792.

Yurkovetskiy, L.A., Pickard, J.M., and Chervonsky, A.V. (2015). Microbiota and autoimmunity: exploring new avenues. Cell Host Microbe *17*, 548–552.

Zhang, X., Zhang, D., Jia, H., Feng, Q., Wang, D., Liang, D., Wu, X., Li, J., Tang, L., Li, Y., et al. (2015). The oral and gut microbiomes are perturbed in rheumatoid arthritis and partly normalized after treatment. Nat. Med. *21*, 895–905.

Zhu, Q., Hou, Q., Huang, S., Ou, Q., Huo, D., Vázquez-Baeza, Y., Cen, C., Cantu, V., Estaki, M., Chang, H., et al. (2021). Compositional and genetic alterations in Graves' disease gut microbiome reveal specific diagnostic biomarkers. ISME J. *15*, 3399–3411.

STAR★METHODS

KEY RESOURCES TABLE

REAGENT or RESOURCE	SOURCE	IDENTIFIER
Antibodies		
CD3	Fisher Scientific	Clone: 17a2Cat: 11-0032-82 RRID: AB_2572431
IL-17a	Fisher Scientific	Clone: ebio17b7 Cat: 25-7177-82 RRID: AB_10732356
CD4	Biolegend	Clone: B2D Cat: 12-6981-80 RRID: AB_493647
IFNy	Fisher Scientific	Clone: XMG1.2 Cat: 45-7311-80 RRID: AB_906239
Foxp3	Fisher Scientific	Clone: R16-715 Cat: BDB563902 RRID: AB_2630318
RORyt	Fisher Scientific	Clone: B2D Cat: 12-6981-80 RRID: AB_10805392
IL-22	Fisher Scientific	Clone: IL22JOP Cat: 17-7222-80 RRID: AB_10597584
TCR$\gamma\delta$	Fisher Scientific	Clone: GL3 Cat: 11-5711-81 RRID: AB_465237
CD45	Fisher Scientific	Clone: 30-F11 Cat: 501129121 RRID: AB_2534954
IL-17f	Fisher Scientific	Clone: eBio18F10 Cat: 501122393 RRID: AB_823149
Lineage negative	Fisher Scientific	Cat: 22-7770-72 RRID: AB_2644066
TCRbeta	Biolegend	Clone: H57-597 Cat: 109240 RRID: AB_2565655
anti-CD3e	BD Biosciences	Cat: BDB553057 RRID: AB_394590
anti-CD28	BD Biosciences	Cat: BDB557393 RRID: AB_396676
anti-IFNy	BD Biosciences	Cat: BDB554409 RRID: AB_398550
anti-IL4	Fisher Scientific	Cat: 14-7041-81 RRID: AB_468410
Bacterial and Virus Strains		
Eggerthella lenta 14A	Turnbaugh Lab	DSM 110907
Eggerthella lenta 28B	Turnbaugh Lab	DSM 110909
Eggerthella lenta DSM 15644	Turnbaugh Lab	DSM 15644
Eggerthella lenta FAA 1-1-60AU	Turnbaugh Lab	DSM 110904
Eggerthella lenta FAA 1-3-56	Turnbaugh Lab	DSM 110906
Eggerthella lenta Valencia	Turnbaugh Lab	N/A
Eggerthella lenta 11C	Turnbaugh Lab	DSM 110905
Eggerthella lenta AB12 #2	Turnbaugh Lab	DSM 110912
Eggerthella lenta AB8 #2	Turnbaugh Lab	DSM 110913

(*Continued on next page*)

Continued

REAGENT or RESOURCE	SOURCE	IDENTIFIER
Eggerthella lenta UCSF 2243	Turnbaugh Lab	DOI: 10.1016/j.chom.2020.04.006
Bifidobacterium adolescentis BD1	Turnbaugh Lab	DOI: 10.1016/j.cell.2020.04.027
Rhodococcus erythropolis strain L88	Balskus lab	DOI: 10.1128/JB.187.8.2582–2591.2005
Primers - See Table S3		
Biological Samples		
Rheumatoid arthritis patient and healthy control stool samples	UCSF Parnassus Rheumatology Clinic	N/A
Ulcerative colitis stool samples	UCSF Colitis and Crohn's Center	N/A
Chemicals, Peptides, and Recombinant Proteins		
DTT	Spectrum	Cat: 40400120-1
HBSS	Life technologies	Cat: 14025126
EDTA	Invitrogen	Cat: AM9260G
Fetal Bovine Serum, heat inactivated	Life technologies	Cat: 10438026
Dispase II	Roche	Cat: 501003345
DnaseI	Sigma	Cat: 10104159001
Collagenase VIII	Sigma	Cat: C2139-500MG
Percoll	VWR	Cat: 89428-524
Sodium Pyruvate (100 mM)	Life technologies	Cat: 11360070
Penicillin-Streptomycin (5,000 U/mL)	Thermo Fisher	Cat: 15070063
MEM Non-Essential Amino Acids	Life technologies	Cat: 11140050
GlutaMAX	Gibco	Cat: 35050061
RMPI 1640	Fisher Scientific	Cat: 11875119
1m HEPES	Fisher Scientific	Cat: NC0734307
Oleanolic acid	Fisher Scientific	Cat: AC456120050
Uvaol	Sigma-Aldrich	Cat: U6628-25MG
Bacto Brain Heart Infusion (broth)	Fisher Scientific	Cat: 237500
L-Arginine	Fisher Scientific	Cat: W381918-1kg
L-Cysteine HCl	Fisher Scientific	Cat: C81020-1000.0
Resazurin	Fisher Scientific	Cat: 199303-5G
Hemin, 5G	Fisher Scientific	Cat: 51280-5G
Menadione (Vitamin K)	Fisher Scientific	Cat: 102259
Chloramphenicol	Fisher Scientific	Cat: #480-045
Thiostrepton	Fisher Scientific	Cat: AAJ6233203
IL-6	VWR	Cat: 575704-BL
TGFβ	Fisher Scientific	Cat: 7666-MB-005
PMA	Fisher Scientific	Cat: AAJ63916MCR
Ionomycyin	Sigma	Cat: I0634-1MG
Cell stimulation cocktail	Fisher Scientific	Cat: 501129036
Golgi plug	Fisher Scientific	Cat: BDB555029
Fixation/Permeabilization Solution Kit	Fisher Scientific	Cat: BDB555028
DSS	Alfa Aesar	Cat: 9011-18-1
Critical Commercial Assays		
IL-17A (homodimer) Mouse Uncoated ELISA Kit	Fisher Scientific	Cat: 5017377
Mouse Lipocalin-2/NGAL DuoSet ELISA	Fisher Scientific	Cat: DY185705
ZymoBIOMICS 96 MagBead DNA Kit	Zymo Reseach	Cat: D4302 / D4306 / D4308
Direct-zol RNA MiniPrep kit	Genesee Scientific Corporation	Cat: 11-331P
RNeasy Micro Kit	Qiagen	Cat: 74004
Rory luciferase assay	Indigo Biosciences	Cat: IB04001-32
iscript	BioRad	Cat: 708891BUN

(*Continued on next page*)

Continued

REAGENT or RESOURCE	SOURCE	IDENTIFIER
Syber select	Life Technologies	Cat: 4472908
RBC lysis buffer	Fisher Scientific	Cat: NC9067514
MojoSort Mouse CD11c Nanobeads	Biolegend	Cat: 480077
Dynabeads untouched mouse CD4 cells	ThermoFisher	Cat: 11415D
Universal plus mRNA kit	Tecan	Cat: 0520-24
LIVE/DEAD Fixable Dead Cell Stain Kit	Life technologies	Cat: L34957
Deposited Datasets		
Metagenomic analysis was performed on samples from an inflammatory bowel disease (IBD) metagenomic survey of Chinese and Spanish (MetaHIT) patients	Qin et al., 2010; Weng et al., 2019	PRJNA429990 and PRJNA431126 (Weng et al. 2019) BioProject: ERA000116 (Qin et al. 2010)
Metagenomic and metabolomic analysis was performed on samples from an inflammatory bowel disease (IBD) metagenomic survey in the PRISM IBD study	Franzosa et al., 2019	Metagenomics: BioProject: PRJNA400072 Metabolomics: NIH Common Fund's Metabolomics Data Repository and Coordinating Center: PR000677
RNA-seq of ileal lamina propria $CD4^+$ cells in germ-free or *E. lenta* monocolonized mice	This paper	GEO: GSE182777
Experimental Models: Organisms/Strains		
Wildtype C57BL/6J mice	Jackson Labs	Cat: 000664
Rorc-/- mice (Rorctm2Litt)	Jody Baron Lab	MGI 104856
IL-10-/- mice (B6.129P2-Il10tm1Cgn/J)	Jackson Labs	Cat: 002251
IL-17a GFP	Jackson Labs	Cat: 018472
Recombinant DNA		
pTipQC plasmid *cgr2*:*WT*	Balskus lab	Koppel et al., 2018
pTipQC plasmid *cgr2*;Y333N	Balskus lab	Koppel et al., 2018
Software and Algorithms		
GraphPad Prism 8	GraphPad Software	https://www.graphpad.com/
FlowJo v10.6.1	TreeStar	https://www.flowjo.com/
R 3.4.0	R	https://r-project.org
Metagenomic Intra-Species Diversity Analysis Subcommands (MIDAS)		https://github.com/snayfach/MIDAS
ElenMatchR	Bisanz et al. 2020	https://github.com/turnbaughlab/ElenMatchR
HS-BLASTN	Chen et al. 2015	https://anaconda.org/bioconda/hs-blastn
ALDEx2	Fernandes et al. 2013	https://www.bioconductor.org/packages/release/bioc/html/ALDEx2.html
Deseq2	Love et al., 2014	https://bioconductor.org/packages/release/bioc/html/DESeq2.html
Other		
Mouse diet: Standard chow diet SPF	Lab diet	Cat: 5058
Mouse diet: Standard autoclaved chow diet (Gnotobiotic studies)	Lab diet	Cat: 5021
Mouse diet: 1% Arg diet	Teklad	Cat: TD.170862
Mouse diet: 3% Arg diet	Teklad	Cat: TD.170863

RESOURCE AVAILABILITY

Lead contact

Further information and requests for resources and reagents should be directed to and will be fulfilled by the Lead Contact, Peter Turnbaugh, Peter.Turnbaugh@ucsf.edu.

Materials availability

This study does not contain newly generated materials

Data and code availability

- All data is available in the main text, the supplemental information, datasets, or deposited as listed below.
- This paper analyzes existing, publicly available data. These accession numbers for the datasets are listed:
(Franzosa et al., 2019) PRISM, LLDeep, and NLIBD cohorts: Metagenomics (BioProject: PRJNA400072). Metabolomics data from supplemental information of (Franzosa et al., 2019) (NIH Common Fund's National Metabolomics Data Repository: PR000677).
(Weng et al., 2019) China cohort: BioProject: PRJNA429990.
(Qin et al., 2010) Spain cohort: EBI: ERA000116.
- RNA-seq data have been deposited at GEO: GSE182777.
- This paper does not report original code.
- Any additional information required to reanalyze the data reported in this paper is available from the lead contact upon request.

EXPERIMENTAL MODEL AND SUBJECT DETAILS

Experimental design

The objectives of these studies were to investigate whether and how a prevalent member of the human gut microbiota which is associated with autoimmune diseases, *Eggerthella lenta*, modulates T helper 17 (Th17) responses and mouse models of chronic inflammation and autoimmunity in a diet-dependent manner. To investigate these questions, we utilized a combination of gnotobiotics, comparative genomics, *in vitro* Th17 skewing assays, mouse models of colitis, metagenomics, and bacterial genetics which are outlined below.

Mice

All mouse experiments were approved by the University of California San Francisco Institutional Animal Care and Use Committee. Housing conditions are specified (either gnotobiotic or SPF as described below). The mice were housed at temperatures ranging from 19-24°C and humidity ranging from 30-70%. No mice were involved in previous procedures before experiments were performed. Mice were assigned to groups to achieve similar age distribution between groups. Both male and female mice were used in these studies.

Gnotobiotic mouse studies

C57BL/6J mice (females and males, ages 6-16 weeks) were obtained from the University of California, San Francisco (UCSF) Gnotobiotics core facility (gnotobiotics.ucsf.edu) and housed in gnotobiotic isolators for the duration of each experiment (Class Biologically Clean) or were housed in Iso positive cages (Tecniplast). Mice were colonized via oral gavage with mono-cultures of *E. lenta* (10^9 CFU/ml, 200 μl gavage) and colonization was confirmed via anaerobic culturing and or qPCR for an *E. lenta* specific marker (elnmrk1) (Bisanz et al., 2020; Koppel et al., 2018). Mice were colonized for 2 weeks unless otherwise stated. For the heat-killed *E. lenta* preparation, 2243 cultures were incubated at 65°C for 15 min to kill bacteria.

SPF mouse studies

C57BL/6J mice (females or males, ages 6-10 weeks) were ordered from Jackson Labs. Mice were orally gavaged with mono-cultures of *E. lenta* strains (10^9 CFU) every other day for 2 weeks and colonization was confirmed with qPCR for an *E. lenta* specific marker (elnmrk1) (Bisanz et al., 2020; Koppel et al., 2018). For CFS SPF experiments, we orally gavaged SPF mice with 200μl CFS where *E. lenta* strain 2243 standardized 48-hour cultures or BHI media controls were centrifuged and filtered through a 0.2 μm filter then through a 3kda filter to select for small molecules <3kDa and concentrated to 2X. *Rorc*$^{-/-}$ (Rorctm2Litt) were generously provided by the Baron lab (UCSF). For repeated gavage in SPF Arg diet experiments *E. lenta* was washed by centrifuging for 10 minutes at 2000rpm then resuspended in the same amount of unconditioned BHI media to remove any CFS. *IL-10*$^{-/-}$ mice were ordered from Jackson Labs (B6.129P2-*Il10*^{tm1Cgn}/J, stock number: 002251) and bred in house. IL-17a GFP mice (C57BL/6-Il17a^{tm1Bcgen}, stock number: 018472) were ordered from Jackson Labs and bred in house.

DSS disease model

For dextran sodium sulfate treatment (DSS) (Alfa Aesar, Cat no. 9011-18-1), single sexed mice (either all male or all female for both experimental and control groups) were given 2% DSS (w/v) *ad libitum* in their drinking water for 6-7 days after mice were colonized with *E. lenta* for 2 weeks prior to disease (either once for monocolonized mice or every other day gavage for SPF animals). SPF mice were additionally gavaged every other day throughout DSS treatment. Mice were monitored for disease progression and weighed daily. Gross signs of toxicity, including hematochezia and weight loss greater than 15% were monitored in this study and mice showing these signs were immediately euthanized. Stools were scored as follows: 0 = normal stool consistency, 1 = soft stool, 2 = blood in stool, 3 = bloody rectum, 4 = prolapsed rectum, 5 = moribund/death (scoring based on (Chassaing et al., 2014)). For the SPF experiments with the 1% and 3% Arg diets, standardized 48 hour *E. lenta* cultures (2243 and 15644) were spun down at

2000 rpm and resuspended in same amount of equilibrated fresh BHI media as *E. lenta* 2243 CFS is sufficient to promote Th17 activation in SPF mice.

IL-10-/- colitis model

For *IL-10*$^{-/-}$ colitis, mice were aged 6 to 10 weeks at the beginning of the experiment with an even distribution between groups (BHI or *E. lenta* strain 2243) and both males and females were used (with similar disease incidence seen between sexes). *IL-10*$^{-/-}$ mice were orally gavaged with 200 μl monocultures of *E. lenta* strains (10^9 CFU) 3 times a week in 3 independent experiments where gavage was carried out for 4, 6, or 10 weeks. Mice were weighed weekly and assessed for rectal prolapse incidence. Mice were sacrificed when they reached the endpoint (rectal prolapse or loss of greater than 15% of starting body weight) outlined in our animal protocol. Lipocalin levels in the colon content were observed via ELISA after 6 or 10 weeks of gavage of mice that remained in the study.

Diets

Custom diets with 1% (TD.170862) or 3% (TD.170863) Arg were purchased from Envigo (Table S2). Otherwise, a chow diet (Lab Diet 5058) was used for SPF mice and an autoclaved chow diet (Lab Diet 5021) was used for the gnotobiotic mice. Diets used for gnotobiotic experiments were either autoclaved or irradiated and vacuum sealed to ensure sterility.

Human subjects

Rheumatoid arthritis and healthy controls subjects

Consecutive patients from the UCSF Parnassus Rheumatology Clinic were screened for the presence of rheumatoid arthritis (RA) based on American College of Rheumatology criteria (Aletaha et al., 2010). RA patients were excluded if they had received prior therapy for RA with a disease-modifying anti-rheumatic drug (DMARD) or biologic therapy. Healthy controls were enrolled in the same clinic and were unrelated volunteer donors. Subjects were 18 years of age or older and both sexes were included in this study. Our study was not powered to assess influence of sex on our phenotypes. After informed consent was signed, patients were provided with toilet hats (Collection Hat, Ability Building Center, NC0441080, Stool Collection Device), sample containers (Collection Vial, Fisher, NC9779954, Sarstedt Brown-Cap Vial) and swabs (Spectrum, 220135, BBL CultureSwab(TM)), cold packs (Fisher Scientific NC0515011) and pre-paid thermal envelopes (Polar Tech 116 Item # 116, Cool Barrier Bubble Economy Next Day) for home collection. Fresh feces were either immediately frozen at home or immediately shipped on frozen ice packs via USPS Priority Express overnight shipping. Samples were placed at -80°C upon receipt. The exclusion criteria applied to all groups were as follows: recent (<3 months prior) use of any antibiotic therapy, current extreme diet (*e.g.*, parenteral nutrition or macrobiotic diet), known inflammatory bowel disease, known history of malignancy, current consumption of probiotics, any gastrointestinal tract surgery leaving permanent residua (*e.g.*, gastrectomy, bariatric surgery, colectomy), or significant liver, renal, or peptic ulcer disease. This study was approved by UCSF Institutional Review Board (IRB #15-17175). DNA was extracted using the MagBead ZymoBIOMICS 96 MagBead DNA Kit (D4302). Bead-beating was done with a Biospec Mini-Beadbeater-96 for 5 minutes.

Inflammatory bowel disease (ulcerative colitis) patient fecal samples

Fecal samples and of adult patients with mild-to-moderate ulcerative colitis (UC; Mayo Score 4-10 (Sands et al., 2019)) enrolled in a trial of fecal microbial transplant (FMT) at the UCSF Colitis and Crohn's Center were used for this study. Ages ranged from 18-64 years of age and both sexes were included in this study. Our study was not powered to assess influence of sex on our phenotypes. This study was approved by the institutional review board of UCSF (IRB #16-20066). Pre-FMT home stool sample collection was facilitated by patients and shipped overnight to the investigators. Upon receipt, samples were frozen at -80°C. Fecal DNA extraction was performed using a modified cetyltrimethylammonium bromide (CTAB) method as previously described (Selvig et al., 2020). Briefly, patient fecal samples were maintained on dry ice while an aliquot (~0.3g) of feces was removed from each sample using a single-use punch biopsy (Integra Miltex, Plainsboro, NJ). Fecal sub-samples were suspended in 500 μl CTAB extraction buffer (5% CTAB in 0.25M phosphate buffer and 1M NaCl) by vortexing and incubating for 15 minutes at 65°C. Phenol:chloroform:isoamyl alcohol (25:24:1) was added and the solution underwent bead-beating at 5.5 m/s for 30 seconds and centrifugation for 5 minutes at 16,000g at 4°C. To improve extraction efficiency, the aqueous phase was collected, and an additional volume of CTAB was added to the sample and heating incubation and bead-beating were repeated. Supernatants from both extractions were pooled (~ 800 μl), mixed with equal-volume chloroform, and centrifuged at 3,000g for 10 minutes. The aqueous phase (~ 600 μl) was transferred to a 96-well plate, combined with twice-volume polyethylene glycol (PEG) and stored overnight at 4°C to precipitate DNA. Samples were then centrifuged at 3,000g for 10 minutes, and the resulting DNA pellets were washed with 300 μl of 70% ethanol, air-dried for 10 minutes, and resuspended in 50-200 μl sterile water.

METHOD DETAILS

Bacterial culturing

E. lenta strain information can be found in the key resources table. *E. lenta* strains were cultured at 37°C in an anaerobic chamber (Coy Laboratory Products) (2%–5% H_2, 20% CO_2, balance N_2). Culture media was composed of brain heart infusion (BHI) media supplemented with L-cysteine-HCl (0.05% w/v), hemin (5 μg/ml), arginine (1%), vitamin K (1 μg/ml), and resazurin (0.0001% w/v) (BHI CHAVR). *E. lenta* strains were previously isolated and sequenced (Bisanz et al., 2020). *R. erythropolis* strain L88 was cultured in

aerobic conditions at 30°C with shaking at 200 rpm in BHI CHAVR. *B. adolescentis* strain BD1 was isolated as described (Ang et al., 2020) and was cultured at 37°C in an anaerobic chamber in culture media comprising brain heart infusion (BHI) media supplemented with L-cysteine-HCl (0.05% w/v), resazurin (0.0001% w/v), hemin (5 μg/ml) and vitamin K (1 μg/ml). For heat-killed (HK) *E. lenta* SPF experiments standardized *E. lenta* strain 2243 cultures were centrifuged 10 min at 2500 rpm, washed with PBS, centrifuged again, resuspended in BHI then incubated for 10 min at 65°C.

Heterologous expression

Cardiac glycoside reductase 2 (*cgr2*) was heterologously expressed in *R. erythropolis* strain L88 as previously described (Koppel et al., 2018). In short, competent *R. erythropolis* were electroporated [2.5 kV pulse (time constant ~4.8)] with pTipQC plasmid carrying the wild-type (*cgr2*:*wt*) or Y333N mutated *cgr2* gene (*cgr2*:Y333N) and transformed cells were selected on Luria-Bertani (LB) chloramphenicol (17 μg/ml) plates. Liquid cultures were grown in BHI CHAVR with 34 μg/ml chloramphenicol to ~0.6 optical density (OD) and then treated with or without Thiostrepton (0.1 μg/ml) to induce expression. CFS was harvested 48 hours later, centrifuged at 2500 rpm for 10 min to pellet the cells and debris then passed through a 0.2 μm syringe filter and used for cell culture assays. Expression induction was verified to be similar levels in the *cgr2*:*wt* and *cgr2*:Y333N plasmids via RT-qPCR for *cgr2* relative to dinB (a control for total *R. erythropolis* load) (Szőköl et al., 2014). For mouse experiments 200 μl *R. erythropolis* CFS or media control (BHI CHAVR with chloramphenicol (34 μg/ml) and thiostrepton (0.1 μg/ml) was gavaged every other day for 2 weeks from the *R. erythropolis* strains (*cgr2*:*wt* or *cgr2*:Y333N). Liquid cultures were prepared as above (see Bacterial culturing section).

Th17 skewing assay

Red blood cell (RBC) lysed mouse splenocytes from male or female C57BL/6J mice were filtered through a 40 μm filter and used for T cell isolation. T cells were isolated via Dynabeads untouched mouse CD4 isolation kit (ThermoFisher) according to kit specifications. Purity of the cells was assessed via flow cytometry for $CD4^+$ cells and ranged from 90-95% $CD4^+$ within the lymphocyte gate. In a 96 well plate pre-coated with anti-CD3 (5 μg/ml, overnight 37°C), equal cell numbers were plated and were treated with bacterial CFS or media controls with pH adjusted to 7 at a concentration of 5% or 7.5% volume/volume. At the same time Th17 skewing conditions were supplied (anti-CD28 (10 μg/ml), TGFβ (0.3 ng/ml), IL-6 (20 ng/ml), anti-IFNγ (2 ng/ml), anti-IL-4 (2 ng/ml) (Huh et al., 2011). Bacterial CFS was harvested from 48 hour stationary cultures where bacterial cells were pelleted (2500 rpm 10 min) and the supernatant was filtered through a 0.2 μm filter to exclude cells from the CFS preparation. Heat treated (HT) CFS were prepared in the same way and then incubated at 95°C for 20 min. 3kDa filtered using Amicon Ultra-15 3kDa spin filters and centrifuging 30 min at 2500 rpm. Isolated $CD4^+$ T cells were developed in Th17 skewing conditions with bacterial CFS present for 4 days at 37°C and then re-stimulated with PMA (50 ng/ml) and ionomycin (1000 ng/ml) overnight, then supernatants were harvested for IL-17a quantification via ELISA. For Figures 2G and 2H, the same set up as above was performed but the CFS was added either at the time of skewing (pre) or after 4 days of skewing during overnight stimulation with PMA (Phorbol 12-myristate 13-acetate) and ionomycin (post). As an additional endpoint we performed flow cytometry on Th17 skewed cells where PMA, ionomycin and Golgi plug were added as previously described for 4-6 hours and then cells were stained for extracellular markers, fixed and then stained for intercellular cytokines (IL-17a). MTT (3-(4,5-dimethylthiazol-2-yl)-2,5- diphenyltetrazolium bromide) proliferation assay cell titer 96 non-radioactive cell proliferation assay (Promega G4000) was used to assay proliferation as per manufacturer's directions. Briefly, 15 μl of dye solution was added, the plate was incubated for 4 hours at 37°C, 100 μl stop solution was added and absorbance was immediately assessed with absorbance at 570 nm.

Rorγ luciferase assay

Human RAR-related Orphan Receptor, Gamma Reporter Assay System (Product # IB04001-32) was purchased from Indigo Biosciences and we performed the luciferase assay according to the manufacturer's instructions with the following specifications. BHI or *E. lenta* CFS were prepared as described above (Th17 Skewing Assay section), dried via speedvac, and reconstituted in Compound Screening Medium (CSM) at a concentration of 10X and was then further diluted to working assay concentrations in CSM. The reporter cell suspensions were plated and pre-incubated for 4 hours prior to treatment with 200 μl of BHI, *E. lenta* 2243 CFS, Ursolic acid (control inverse agonist), or no treatment. Cells were incubated 22 hours with treatments before treatment media was removed and luminescence was determined with a Cytation5 imaging reader.

Antigen specificity experiments

We modeled our antigen presentation assays on previously published assays (Tan et al., 2016). Dendritic cells (DCs) were isolated with anti-CD11c magnetic beads (MojoSort Mouse CD11c Nanobeads) from C57/BL6J spleens and loaded with mock (BHI), *E. lenta*, or *B. adolescentis* lysates. Lysates were prepared from monocultures by autoclaving at 121°C for 20 min. Protein levels were quantified via BCA assay and 250μg/mL of protein was loaded to the isolated DCs overnight. SPF C57/BL6J mice were gavaged every other day with BHI, *E. lenta*, or *B. adolescentis* for 2 weeks. Small intestinal tissue from these mice was processed as described in the lamina propria lymphocyte isolate section with the exclusion of the percoll gradients and T cells were isolated as described in the Th17 skewing section with Dynabeads untouched mouse CD4 isolation kit (ThermoFisher). These isolated T cells were plated with the lysate loaded DCs at a ratio of 1:10 (DC:T) and 20U/ml IL-2 was added and incubated 20-24 hours with Golgi Plug added in

the last 12 hours. After the incubation cells were stained for extracellular markers (live/dead, CD3, CD4) and intracellular cytokines (IL-17a) as described in the flow cytometry section. Experiments were performed with a total of 4 mice per group and 2-4 biological replicates (wells) per mouse.

ELISAs

To measure the levels of secreted IL-17a from the Th17 cell culture assay we utilized the mouse IL-17a (homodimer) ELISA (ThermoFisher) according to the kit instructions, where 100 μl of cell culture media was loaded into ELISA. Raw values for IL-17a ELISAs are listed in Data S3. To measure lipocalin levels in the colon contents 10 mg of colon content was resuspended in 200 μl of 0.1% tween20 in PBS, vortexed for 20 min at speed 8-9, spun for 10 min at 12,000 rpm to pellet debris. The supernatant was collected and used for a lipocalin ELISA (Mouse Lipocalin-2/NGAL DuoSet ELISA, R&D systems) according to the manufacturer's instructions, where 100 μl of the supernatant was loaded onto a coated ELISA plate. Absorbance for ELISA was measured at 450 nm and the blank background signal was subtracted.

Lamina propria lymphocyte isolation

Lamina propria lymphocytes (LPLs) were isolated with modifications of previously described methods (Atarashi et al., 2011; Kubinak et al., 2015; Round et al., 2011). Briefly, small intestinal (SI) Peyer's patches were excised and colons and the lower $^{2}/_{3}$ of the SI tissue were splayed longitudinally with mucus removed and stored in complete RPMI (10% fetal bovine serum, 100 units per ml penicillin and streptomycin, β-mercaptoethanol, glutamax, sodium pyruvate, hydroxyethyl piperazineethanesulfonic acid (HEPES) and non-essential amino acids). Media was removed by filtering through a 100 μM filter, and remaining tissue incubated in 1X Hank's Balanced Salt Solution (HBSS -without Ca^{2+} and Mg^{2+}) containing 5 mM ethylenediaminetetraacetic acid (EDTA) and 1 mM DL-Dithiothreitol (DTT) for 45 min at 37°C on a shaker (200 rpm). Supernatant were filtered through a 100 μM filter, and remaining tissue was incubated for 45 min (colon) or 35 min (SI) at 37°C on a shaker in a solution containing 1X HBSS containing 5% (v/v) fetal bovine serum (GIBCO heat inactivated), 1 U/ml Dispase (Sigma), 0.5 mg/ml Collagenase VIII (Sigma), and 20 μg/ml DNaseI (Sigma). The vortexed supernatant was filtered over a 40 μm cell strainer into 1X PBS. Cells were subjected to a Percoll (VWR) gradient (40%/80% [v/v] gradient) and spun at 2000 rpm for 20 min with no brake and no acceleration. Cells at the interface were collected, washed in 1X PBS and prepared for flow cytometry analysis as described in the next section.

Flow cytometry

Lymphocytes were isolated from the colonic and SI lamina propria as described above. Spleen cells were prepped through gentle mashing with a syringe plunger. Spleen cells were treated with 1X RBC Lysis Buffer (Biolegend) to lyse and remove red blood cells. Surface staining for lymphocytes was done in staining buffer (1X HBSS (Corning) supplemented with 10 mM HEPES (Fisher Scientific), 2 mM EDTA (Invitrogen), and 0.5% (v/v) fetal bovine serum (GIBCO heat inactivated)) for 20 min at 4°C. Cells were then washed twice in supplemented 1X HBSS and enumerated via flow cytometry. The following antibodies were used: anti-CD3 (17A2, Fisher Scientific), anti-TCRβ (H57-597, Biolegend), anti-CD4 (GK1.5, Biolegend), and live/dead staining was performed using LIVE/DEAD Fixable Dead Cell Stain Kit (Life Technologies). For intracellular staining, cells were first stimulated with ionomycin (1000 ng/ml), PMA (50 ng/ml), and Golgi Plug (1 μl/sample) (BD Bioscience) 4-6 hours or overnight at 37°C. Alternatively, cells were stimulated with a cell stimulation cocktail (Fisher Scientific) containing PMA and ionomycin according to the manufacturer's instructions, and Golgi plug was added. Cells were surface stained, washed, and then fixed/permeabilized in 100 μl fixation and permeabilization (Perm) buffer (BD Bioscience). Cells were washed twice in Perm/Wash buffer (BD Bioscience) and then stained for intracellular cytokines with the following antibodies: anti-IFNγ (XMG1.2, Fisher Scientific), anti-IL17a (ebio17B7, Invitrogen), Rorγt (B2D, ebioscience). Cells were washed twice in Perm/Wash buffer and then placed in staining buffer for flow cytometry analysis. Gating cell populations was done using isotype and single stain controls. Gating strategies and which figures they correspond to are outlined in Figure S2. Live/dead staining or forward or side scatter (FCS, SSC) occasionally revealed a high death incidence in some lamina propria lymphocyte isolations after PMA and ionomycin stimulation. These samples were removed from our analysis of immune cells as they had high levels of non-specific background fluorescence and too few cells to analyze. Fold-change of Th17 cells or IL-17 is relative to the mean of the appropriate control. The flow cytometry data were collected with a BD LSR Fortessa and analyzed with FlowJo software (version 10.6.1) and a list of all antibodies are included in the key resource table.

Histology

1 cm sections of the distal colon were collected for histological processing from DSS treated mice. Samples were fixed in formalin for 24 hours and then stored in 70% ethanol. Samples were processed by the UCSF Biorepository and Tissue Biomarker Technology Core. Tissues were embedded in wax and 4 μm cross-sections were hematoxylin and eosin (H&E) stained.

E. lenta comparative genomics

To identify shared genetic regions of IL-17a inducing *E. lenta* strains which were also excluded from non-IL-17a inducing *E. lenta* strains we utilized ElenMatchR (github.com/turnbaughlab/ElenMatchR) (Bisanz et al., 2020). Briefly, gene presence/absence was used as the input variable for a random forest classifier against user-provided phenotypes or traits, in this case induction or non-induction of IL-17a by *E. lenta* strains. With these classifications, we performed comparative genomics using ElenMatchR (80%

coverage and 80% minimum identity 3 replications of the random forest analysis and 1000 trees generated in the model) to determine genomic regions shared between the 4 inducing strains and absent from the 6 non-inducing strains.

RNA/DNA isolation and qPCR

Ileal segments from GF or *E. lenta* monocolonized mice were harvested and RNA was extracted with Direct-zol RNA MiniPrep kit (Zymo) according to manufacturer instructions for tissue RNA isolation. Tissue was homogenized with a mortar and pestle and DNase treatment was performed on columns. RT-PCR was performed with iScript (BioRad) using ~300 ng RNA and RT-qPCR using SYBR select. DNA was extracted from mouse cecal samples to quantify levels of *E. lenta* or Cgr2 with the ZymoBIOMICS 96 MagBead DNA Kit according to manufacturer's instructions. Briefly, samples were weighed out (~50 mg), lysed, disrupted for 5 minutes in Biospec beadbeater, washed, and eluted in 50 μl. For quantification of *cgr2* from human fecal samples qPCR was performed with ~20 ng gDNA using SYBR select and levels were normalized to input μg of DNA. For *E. lenta* quantification DNA was extracted from mouse cecal content (~50 mg) or human fecal samples and *E. lenta* specific primers (elnmrk1) were used with SYBR select with 2 μl of gDNA (~20 ng). Primers are listed in Table S3 including primers from the following studies (Atarashi et al., 2015; Bisanz et al., 2020; Dumas et al., 2018; Geng et al., 2019; Haiser et al., 2013; He et al., 1998; Hu et al., 2014; Kawashima et al., 2012; Koppel et al., 2018; Lee et al., 2016; Liu et al., 2019; Middleton et al., 2009; Moore-Smith et al., 2017; Szőköl et al., 2014; Tachiiri et al., 2003; Ueda et al., 2012; Wei et al., 2018; Yang and Xu, 2016).

RNA sequencing

Ileal lamina propria cells were isolated as described in the previous section (Lamina Propria Lymphocyte Isolation) and CD4 T cells were isolated using Dynabeads untouched mouse CD4 isolation kit (ThermoFisher) as described in the previous section (Th17 Skewing Assay) with the modification of performing the isolation procedures twice to assure a pure $CD4^+$ population. Purity of isolated cells was assessed with flow cytometry and 99% of cells were confirmed to be CD4+. RNA was isolated using a Qiagen RNeasy Micro kit according to manufacturer's instructions with the following specifications. Isolated $CD4^+$ cells were stored in RNAlater at -80°C, cells were thawed on ice, and pelleted by centrifugation prior to lysis buffer addition. Cells were lysed by vortexing for 20 seconds. RNA quality was assessed with nanodrop and bioanalyzer before library preparation with Universal plus mRNA kit and sequencing with HiSeq4000 by the UCSF Institute for Human Genetics core facility. Data were analyzed with DEseq2 (Love et al., 2014) in R.

RP-HPLC

5ml 48 hour turbid cultures of *E. lenta* strains 2243 and 1356 were grown anaerobically and CFS were obtained as previously described (Bacterial Culturing and Th17 Skewing Assay sections). CFS were further filtered through a 3kDa filter using Amicon Ultra-15 3kDa spin filters and centrifuging 30 min at 2500 rpm. 1.5ml of the filtered CFS were dried using a speedvac and reconstituted in sterile water to a 10X concentration. RP-HPLC was performed with the following settings with a BDS C8 hypersil column (28205_154630 BDS Hypersil C8 150X4.6). Water and 100% methanol gradient: 2min: 80% water, 20% methanol, 6 min: 5% water, 95% methanol, 9 min: 5% water, 95% methanol, 9.5 min: 80% water, 20% methanol. A total of 7 fractions were collected with the 1st fraction a short (5 sec) wash out followed by 6 fractions in 1.5 time slices starting at 1 min and ending at 9 min. These fractions were then dried via speedvac and resuspended in RPMI for testing in our Th17 skewing assay and LCHRMS analysis.

LCHRMS and analysis

RP-HPLC fraction 5 from BHI, *E. lenta* 2243, and *E. lenta 1356* were desalted using solid phase extraction (Agilent Bond Elut C18). Briefly, SPE cartridges were conditioned with two volumes methanol and water, HPLC fractions samples were diluted 10X with water then applied to SPE cartridges. Samples were washed with two volumes of water, and compounds of interest were eluted in 400 uL MeOH. The MeOH eluent was dried under vacuum and nitrogen, re-dissolved in 150 uL MeOH and stored at -80C for Liquid Chromatography High-Resolution Mass Spectrometry (LCHRMS) analysis. Untargeted LCHRMS analysis was performed on a Sciex Exion UPLC equipped with a BDS C8 hypersil column (Thermo, 150 x 4.6 mm, particle size 5 u) and coupled to a Sciex TripleTOF 6600+ operated in both positive and negative mode electrospray ionization with IDA acquisition of MS2 (accumulation time 0.25 s, collision energy 30V (15V spread), acquisition window 100-2000 Da). A gradient of 0% - 100% acetonitrile over 9 min was used for compound separation.

Feature-based molecular networking analysis (FBMN) (Nothias et al., 2020) was performed on shared MS/MS fragments across all metabolite features to determine the relationship between metabolite features detected in our HPLC fraction mixtures. Raw mass spectrometry data was preprocessed using MzMine2 (Katajamaa et al., 2006; Pluskal et al., 2010) for feature detection, chromatogram building, peak deconvolution, isotope grouping, gap filling, and alignment. The resulting intensity-based metabolite feature matrix and MS2 mgf files were used for further statistical and network analyses in Metaboanalyst (Pang et al., 2021) and GNPS (Wang et al., 2016).

To summarize, a molecular network was created using the online workflow (https://ccms-ucsd.github.io/GNPSDocumentation/) on the GNPS website (http://gnps.ucsd.edu). The data was filtered by removing all MS/MS fragment ions within +/- 17 Da of the precursor m/z. MS/MS spectra were window filtered by choosing only the top 6 fragment ions in the +/- 50Da window throughout the spectrum. The precursor ion mass tolerance was set to 2.0 Da and a MS/MS fragment ion tolerance of 0.5 Da. A network was then created where edges were filtered to have a cosine score above 0.7 and more than 6 matched peaks. Further, edges between two nodes were kept in the network if and only if each of the nodes appeared in each other's respective top 10 most similar nodes. Finally,

the maximum size of a molecular family was set to 100, and the lowest scoring edges were removed from molecular families until the molecular family size was below this threshold. The spectra in the network were then searched against GNPS' spectral libraries. The library spectra were filtered in the same manner as the input data. All matches kept between network spectra and library spectra were required to have a score above 0.7 and at least 6 matched peaks. The molecular networks were visualized using Cytoscape software (Shannon, P. et al. Genome Res. 13, 2498-2504 (2003)).

Following FBMN, Network Annotation Propagation (NAP) (da Silva et al., 2018), MS2LDA (Wandy et al., 2018), Dereplicator (Mohimani et al., 2018) and MolNetEnhancer (Ernst et al., 2019) were used to assign chemical classifications to the metabolite features.

Metagenomic data analysis

Metagenomic analysis was performed on samples from an inflammatory bowel disease (IBD) metagenomic survey of Chinese, Spanish (MetaHIT), and PRISM (the Prospective Registry in IBD Study at MGH) studies (Franzosa et al., 2019; Qin et al., 2010; Weng et al., 2019). Shotgun metagenomic reads were analyzed with an implementation of Metagenomic Intra-Species Diversity Analysis Subcommands (MIDAS) (Nayfach et al., 2016) designed for a Unified Human Gastrointestinal Genome (UHGG) collection of 286,997 isolate genomes and metagenome assembled genomes from the human gut environment. Presence of *E. lenta* in a given sample was established when reads mapped to 15 *E. lenta* single-copy universal genes (HS-BLASTN) (Chen et al., 2015), with at least 75% alignment coverage. Because species read counts are by nature compositional, species relative abundance between sample types was determined by centered-log ratio (clr) transformation of species raw read counts, and subsequent Kruskal-Wallis test for significance using ALDEx2, run with 128 Monte Carlo samples of the Dirichlet distribution for each sample (Fernandes et al., 2013, 2014; Gloor et al., 2017). In addition, rank relative abundance of *E. lenta* was assessed by ranking all species by their median relative abundance in a given disease type. When analyzing differences between groups after combining the Spanish and Chinese cohorts, a generalized linear model was used to adjust for dataset, and *p-value*s reported as a t-test on the glm coefficient. In addition, rank relative abundance of *E. lenta* was assessed by ranking all species by their median relative abundance in a given disease type.

To assess the gene content of *E. lenta* positive individuals in the PRISM cohort, shotgun metagenomic reads were aligned to a MIDAS created pangenome of *E. lenta* genes clustered at 99% nucleotide identity. Copy number of *cgr2* was established by dividing aligned *cgr2* reads by the full length of *cgr2*. This number was then normalized by the read coverage of 15 single-copy universal genes in the same sample to estimate copy number per cell. Presence of *cgr2* in *E. lenta* positive individuals was established if at least 0.35 gene copies per cell were present in a sample.

QUANTIFICATION AND STATISTICAL ANALYSIS

To control for expected experimental variation we describe Th17 levels or IL-17a levels as fold-change where fold-change of Th17 or IL-17a levels is relative to the mean of the appropriate control. Statistical analyses were performed using GraphPad Prism software (Version 8). ANOVA with Tukey's, Dunnett's, or Holm Sidak multiple comparison test was used for the parametric analysis of variance between groups, and unpaired Welch's t-tests were used for pairwise comparisons. All statistical tests are described in the figure legends and are two-tailed unless otherwise stated. A one-sided Fisher's exact test between *cgr2* prevalence was used to compare healthy and RA. When analyzing differences between groups after combining the Spanish and Chinese cohorts, a generalized linear model was used to adjust for the dataset, and *p-value*s reported as a t-test on the glm coefficient. Two-way ANOVAs with Sidak multiple comparisons tests were used to compare disease scores and weights over time. Outliers were removed as determined by ROUT (Q = 10%) or Grubb's (alpha = 0.2) methods. Numbers (*n*) are stated and displayed as individual points on plots. Definitions of center, and dispersion and precision measures are stated in figure legends which include mean±SEM, Tukey box and whisker plots, volcano plots, heatmaps, and Kaplan-Meier curves.